NTNU – Trondheim
Norwegian University of
Science and Technology

Reduced Order Observer Design for Managed Pressure Drilling

Ulf Jakob Flø Aarsnes

Master of Science in Engineering Cybernetics
Submission date: June 2012
Supervisor: Ole Morten Aamo, ITK

Norwegian University of Science and Technology
Department of Engineering Cybernetics

Abstract

This thesis presents a dynamic model of the surge/swab pressure fluctuations in a drilling well induced by the vertical movement of the drill string. The model is given by a coupled set of Partial Differential equations describing: 1. the pressure dynamics in the annulus under unsteady Couette flow with a pressure gradient, 2. The movement of the elastic drill string coupled with the pressure dynamics through viscous friction and mud displacement. It is shown how the model can be simplified to a linear system and under what conditions this simplification hold. Using the Laplace transform and appropriate boundary conditions the transfer function of the linear model is derived. The model uses the heave disturbance and controlled flow into the drilling well as inputs, and the measured topside pressure and controlled down-hole pressure as output. It is also shown how the system may be discretized to obtain a dynamic system given by a set of Ordinary differential equations. The error introduced by the discretization is analysed in the frequency domain. Then, the discretized models with varying number of control volumes are used for Kalman filter design. The performance of the Kalman filter when the well is subjected to the heave disturbance is compared over different number of control volumes for typical values of measurement noise and heave velocity. Finally, it is shown that improved performance of the Kalman filter for a fixed order can be obtained by designing the Kalman filter on a high order discretization and then utilizing frequency weighted model reduction.

Abstract

Denne hovedoppgaven presenterer en dynamisk modell av trykkendringer i en borebrønn laget av vertikal bevegelse av borestrengen. Modellen er gitt av et sett av koblede PDEer som beskriver: 1. trykkdynamikken i brønnens annulus under ustødig Couette flyt med en trykkgradient, 2. Bevegelsen til den elastiske borestrengen som er koblet med trykkdynamikken gjennom viskøs friksjon og fortrengning av boreslam. Det blir vist hvordan modellen kan forenkles til et lineært system og under hvilke forutsetningen denne forenklingen holder. Ved bruk av Laplacetransformen og innsetting av hensiktsmessige grensebetingelser så utledes transferfunksjonen til det lineære systemet. Den resulterende modellen bruker hiv forstyrrelsen og kontrollert flyt inn i borebrønnen som inngang, og det målte trykket i toppen av brønnen, samt trykket i bunnen av brønnen som utgang. Det blir så vist hvordan modellen kan diskretiseres for å oppnå et system gitt ved et sett av ordinære differensialligninger. Modellfeilen som blir introdusert av diskretiseringen blir analysert i frekvensdomenet. Det diskretiserte systemet, med varierende antall kontrol volum, blir så brukt til å designe Kalmanfiltre. Kalmanfiltrenes ytelse blir sammenlignet og det blir vist hvordan man kan bruke frekvensvektet modellreduksjon for å oppnå et Kalmanfilter av lav orden med bedre ytelse enn om de skulle vært designet direkte med en modell med få kontrol volum.

Contents

List of Figures

List of Tables

Abbreviations

Nomenclature: The Hydraulic Well Model

A_a = Annulus cross-sectional area$[m^2]$

A_b = Drill String cross-sectional area$[m^2]$

A_p = Openhole section cross-sectional area$[m^2]$

ΔA_a = change in annulus cross-sectional area around the BHA$[m^2]$

ΔA_p = change in drill string cross-sectional area$[m^2]$

β = Bulk modulus of the drilling mud

β_p = Youngs modulus of the drill string

$\bar{\beta}_a$ = Effective bulk modulus in the annulus

$\bar{\beta}_b$ = Effective bulk modulus in the openhole section

c_a = Sonic velocity of the mud in the annulus $[m/s]$

c_b = Sonic velocity of the mud in the openhole$[m/s]$

c_p = Sonic velocity of the mud in the drill string$[m/s]$

C_d = Discharge coefficient, dimensionless

E_i = Youngs modulus of the drill string [Pa]

E_o = Youngs modulus of the formation around the well [Pa]

$f_a(v_a, v_p)$ = Viscous drag acting on the mud in the annulus [Pa/m]

$f_b(v_b)$ = Viscous drag acting on the mud in the openhole section [Pa/m]

$f_p(v_a, v_p)$ = Viscous drag acting on the drill string [Pa/m]

F_a = Forces acting on the mass in a control volume$[N]$

g = Acceleration of gravity $[m/s^2]$

k_a = Linear viscous friction coefficient of mud in annulus w.r.t. mud velocity $[\frac{kg}{m^3 * s}]$

k_b = Linear viscous friction coefficient of mud in openhole $[\frac{kg}{m^3 * s}]$

k_d = Linear viscous friction coefficient of mud in annulus w.r.t. pipe velocity $[\frac{kg}{m^3 * s}]$

$k_p =$ Linear viscous friction coefficient of drill string w.r.t. mud velocity $[\frac{kg}{m^3 * s}]$

$K_1 =$ Hoop-strain coefficient, dimensionless

$l^j =$ Length of the jth control volume of the annulus and drill string $[m]$

$l_b^j =$ Length of the jth control volume of the openhole section $[m]$

$L =$ Length of the annulus and drill string $[m]$

$L_b =$ Length of the openhole section $[m]$

$N =$ Number of control volumes in the annulus and drill string

$N_b =$ Number of control volumes in the openhole section

$p_a =$ Annulus mud pressure $[Pa]$

$p_b =$ Openhole mud pressure $[Pa]$

$p_p =$ Drill string pressure $[Pa]$

$p_c =$ Mud pressure at the top of the annulus $[Pa]$

$p_r =$ Mud pressure around the BHA $[Pa]$

$q_c =$ Volumetric flow into the top of the annulus: $q_c = q_{bpp} - q_{choke} [m^3/s]$

$q_{bpp} =$ Volumetric flow through the back-pressure pump $[m^3/s]$

$q_{choke} =$ Volumetric flow through the topside choke $[m^3/s]$

$r_i =$ Inner radius of the annulus $[m]$

$r_o =$ Outer radius of the annulus $[m]$

$t =$ Time, seconds

$u_i =$ Displacement of the inner radius of the annulus $[m]$

$u_o =$ Displacement of the outer radius of the annulus $[m]$

$v_a =$ Velocity of the mud in the annulus $[m/s^2]$

$v_b =$ Velocity of the mud in the openhole section $[m/s^2]$

$v_d =$ Velocity of the drill string at the top of the well $[m/s^2]$

$v_p =$ Velocity of the drill string $[m/s^2]$

$v_r =$ Velocity of the mud around the BHA $[m/s^2]$

$x =$ Position in the annulus and drill string, $x = 0$ is at the BHA

$x_b =$ Position in the openhole section, $x = 0$ is at the bottom-hole

$\alpha, \alpha_1, \alpha_2, \alpha_3, \alpha_4, \alpha_5 =$ Parameters dependent on the annulus diameter ratio

$\mu =$ Mud viscosity$[m/s]$

$\mu_i =$ Poissons ratio for drill string

$\mu_o =$ Poissons ratio for formation

$\rho =$ Mass density of the mud $[kg/m^3]$

$\rho_p =$ Mass density of the drill string $[kg/m^3]$

Subscripts

$a =$ properties in the annulus
$b =$ properties in the openhole section
$p =$ properties in the drill string

Superscripts

$j =$ properties of the jth control volume in the discretized model
$s =$ the steady state value of the property at $t = 0$
$- =$ upstream properties
$+ =$ downstream properties

Nomenclature: Analysis of Simplified Model

$C_1, C_2 =$ Constants of integration for the one dimensional damped wave equation
$i = \sqrt{-1}$
$p_{bit} =$ Pressure in the annulus at the BHA [Bar]
$p_c =$ Pressure in at the top of the annulus [Bar]
$s =$ The laplace transform variable
$y_p =$ Particular solution of the inhomogeneous damped one dimensional wave equation
$\gamma =$ Convenience variable in the solution of the damped one dimensional wave equation
$\omega =$ Frequency $[rad/s]$
$\omega_{r,j} =$ Frequency of the jth resonance peak $[rad/s]$

Subscripts

$t =$ shorthand for $\partial/\partial t$
$x =$ shorthand for $\partial/\partial x$

Nomenclature: Estimator Design

$A, b_1, C_1, C_2, D_{11} =$ System matrices of the discretized plant
$A_\epsilon =$ Modified schur system matrix
$F^N =$ Kalman filter designed with $\tilde{P}^N$
$P =$ Irrational transfer function matrix
$P_{11}, P_{12}, P_{21}, P_{22} =$ Irrational transfer functions
$\tilde{P} =$ Transfer function matrix of realization of the discretized LTI system
$Q =$ Covariance of the unweighted disturbance
$R =$ Covariance of the measurement noise
$S =$ Cross-covariance of the measurement noise with the disturbance
$T_{i,j} =$ Transfer function matrix from inputs j to outputs i
$v_1, v_2, v_3 =$ Measurement noise in the Kalman filter design
$w =$ Weighted disturbance input vector in the Kalman filter design
$\tilde{w} =$ Unweighted disturbance input vector in the Kalman filter design
$W_d =$ Disturbance frequency weighting function
$y =$ Vector of measurement signals available to the Kalman Filter
$z =$ Estimated variable in the Kalman filter design
$\Sigma_c =$ Controllabillity Grammian
$\Sigma_o =$ Observabillity Grammian

Superscripts

$N =$ number of control volumes in discretization
$n =$ order of LTI system
$\hat{} =$ estimation of variable
$* =$ the complex conjugate transpose
$' =$ the transpose

Glossary

BHA	Bottom Hole Assembly, the end of the drill string
cosh	Hyperbolic cos, $\cosh(x) = \frac{e^x + e^{-x}}{2}$
CV	Control Volume
$E\{x\}$	Expected value of x
LTI	Linear Time Invariant
MPD	Managed Pressure Drilling
ODE	Ordinary Differential Equation
Openhole	The part of the well that is below the drill string.
PDE	Partial differential equation
sinh	Hyperbolic sin, $\sinh(x) = \frac{e^x - e^{-x}}{2}$
tanh	Hyperbolic tan, $\tanh(x) = \frac{e^x - e^{-x}}{e^x + e^{-x}}$

Chapter 1

Introduction

1.1 MPD and the Heave Attenuation Problem

In drilling operations performed in the oil and gas industry a fluid called mud is pumped down through the drill string and flows through the drill bit in the bottom of the well, see Fig. 1.1.

If the pressure in the mud at the bottom of the well is too low the well can collapse trapping the drill string, and if the pressure exceeds a certain threshold it can fracture the well. Hence, it is important to control the mud pressure in the well. In Managed Pressure Drilling (MPD) operations this is achieved by sealing the well and releasing mud from the well through a control choke. A back pressure pump allows the pressure to be controlled even when the main pump is stopped. Thus, the pressure in the bottom of the well can be regulated to a desired set-point. This approach has proven successful when drilling from stationary platforms and results on MPD control can be found in papers such as [20],[7]. MPD from floating drilling rigs, however, still face significant challenges due to the wave induced vertical motion of the floating drilling rig (known as heave). During normal drilling the heave motion of the drilling rig is decoupled from the drill string by compensation techniques. However, when the drill string is to be extended by a drill string connection it is rigidly connected to the floater. It will then act as a piston in the well creating pressure oscillations which may exceed the upper or lower pressure thresholds one wishes to enforce. It is therefore desirable to utilize active control of the topside choke to compensate for the pressure changes due to the heave motion. In this scenario, the main pump is disconnected and there is no flow between the annulus and the drill string (the drill bit is equipped with a one-way valve which prevents back flow from the annulus into the drill string.) Hence the dynamics of interest is the pressure dynamics in the annulus.

The pressure dynamics in the annulus can be described by a hydraulic transmission line model given by a set of hyperbolic PDEs. This system is continuous in time and space and its governing equations include differential relations in both time and space which is what makes them PDEs. That the PDEs are hyperbolic means that information travels at a finite velocity which in this case is the sonic velocity of the given medium. The PDEs

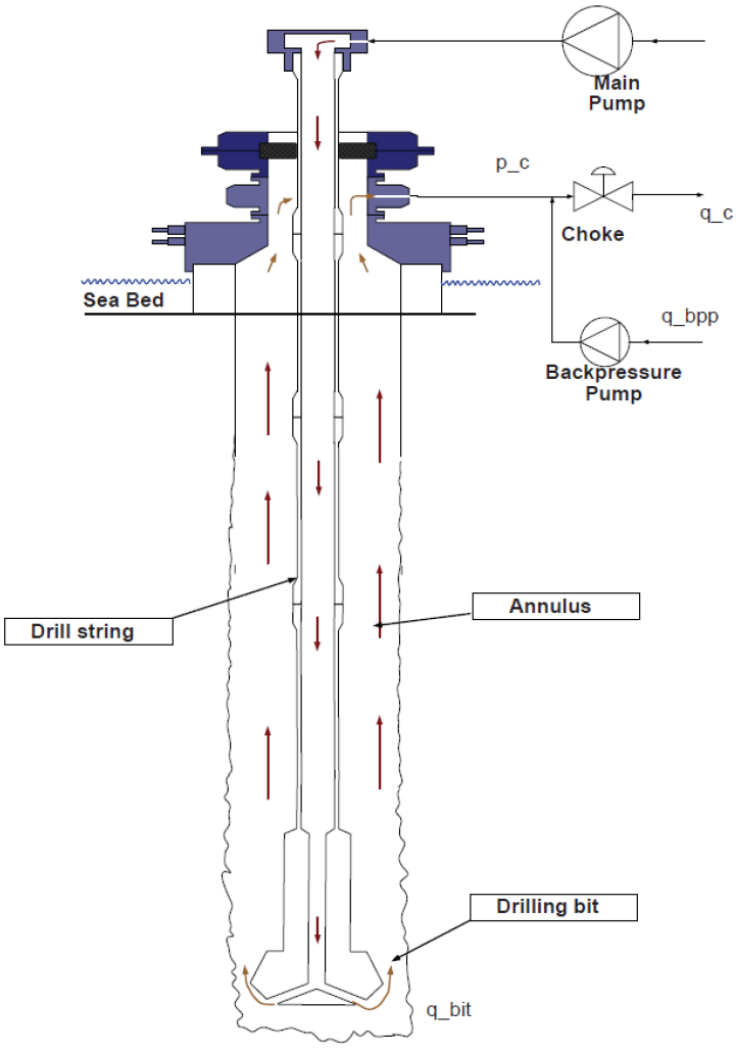

Figure 1.1: Well configuration for MPD. Shown by courtesy of Statoil ASA.

can be discretized w.r.t. space which yields a set of ODEs. Linearising these yields a finite dimensional LTI system which allows for the use of standard LTI controller and estimator design techniques. But, to maintain the property of finite velocity of the information, a high order discretization may be required which again results in high order estimators and controllers. This necessitates the use of model reduction techniques to reduced the order of the designed LTI systems while maintaining performance.

1.2 Contribution

The contribution of this thesis is twofold: one is towards the solution of the heave attenuation problem in MPD, and the other is a theoretical contribution in using an irrational transfer function directly in the performance evaluation of the designed estimator.

Chapter 2 gives the main contribution to the heave attenuation problem. In this chapter it is shown that the modelling of the pressure dynamics in the well in earlier works on the heave attenuation problem is incomplete. Then a new and improved model, based on a seminal work which have been verified in tests and is also used in industry, is proposed. Potential simplifications of the model are also proposed and the resulting assumptions are explicitly given.

The other contribution comes from the derivation of the transfer function of the simplified model in closed form. It is shown in chapter 4 how this transfer function is a valuable tool in evaluating performance of controllers and estimators designed with a LTI discretization of the model.

1.3 Outline

The Thesis is organized in the following way: the hydraulic well model is presented, and then discretized in Chapter 2. In chapter 3, the frequency response of the linearised model is derived. Finally, in chapter 4 the results are applied the design of a low order estimator of the bottom-hole pressure.

Chapter 2

The Hydraulic Well Model

2.1 Background

In [21] a simple one control volume was used to develop a controller for attenuating the disturbance due to floater heave in a drilling well. The model was originally developed in [14] where it was used for pressure estimation under normal drilling conditions, i.e. it only had to consider very slow dynamics. The heave dynamics, however, was to fast for the one control volume model and hence the full scale tests conducted with the controller from [21] failed.

A general model for the pressure dynamics in the wellbore based on the hydraulic transmission line from [3] was presented in [16]. This model considered among other things the heave disturbance, but was not created specifically for controller design. It included non-linear relations such as a non-newtonian Rheological model and a state machine to model the thixotropy of the drilling mud. The model did not consider the effect of drilling mud clinging to the moving drill string (as by the no slip condition). This effect is well documented in experiments and papers such as in [23] and in [12] where it is concluded that: "*The moving pipe walls greatly influence the mud velocity in the annulus (and, hence, the pressure surge).*" Hence this model should be considered incomplete and will fail in cases where the drilling mud is thick[1].

This model was used in distributed form in [8] and [9], and presented in discretized form in [10]. It was also used for controller design in [17].

2.1.1 Surge and Swab Pressure Models

Surge and Swab pressure evaluation is a well researched field of petroleum engineering. The problem is usually presented in the context of running or pulling pipes in a borehole with an annulus that is open topside, but most of the conclusions should hold for MPD as well.

[1] I.e. the mud has a high viscosity, and/or high yield stress in the case of a Bingham Plastic. This is discussed further in section 3.1.3

In a seminal paper [12], Burkhardt presented approximate equations to compute surge pressure for Bingham plastic fluid with comparisons to experimental results. The study identified the three major causes of surge and swab pressure as: viscous shear, breaking the gel strength and pipe acceleration. The difficulty of calculating the viscous shear stress in the non-Newtonian mud due to the moving drill string was noted. Burkhardts model as well as one due to Fontenot and Clark [4] are so called *steady state* models, where the drilling mud is perfectly displaced by the pipe motion and fluid pressures are calculated to be consistent with frictional pressure drops.

One of the early studies on the unsteady-state flow model was presented in [18]. The paper showed that fluid compressibility has a major effect on pressure surge and studied the effects of the different physical parameters of the well. They concluded that "*calculation of surge pressure on the basis of steady state flow is inadequate*".

In [23], Mitchell presented a dynamic flow model to predict surge pressure. The model showed good agreement when compared to field data. In this study factors such as elasticity of the drill string and borehole formation was considered. It was also concluded that:*In deep wells, fluid compressibility is important.* In [24], it was concluded that Mitchells dynamics Surge/Swab model "*demonstrates excellent agreement with the [..] measurements collected during field tests*". This model has also been adapted by industry [1].

A complicating issue with unsteady flow models have been the viscous friction between the moving drill string and a non-Newtonian drilling mud. In [25] it were stated that "*There has been no reported simple analytical solution and application of the unsteady Couette flow phenomena to solve fluid flow problems when a concentrically placed cylinder is in motion.*" Although the motion equations were analytically solved for non-Newtonian power-law fluids in this paper, the pressure gradient were given by an implicit relation with regards to the velocity of the fluid and the drill string. This means that the equations of motion are given in a so-called semi-analytical form, and could therefore not be used directly in ODE-based dynamic models [6]. In [6] a single flow equation, explicit in the pressure gradient, that approximates the analytical solutions for Bingham Plastic-fluids in the annulus were given. In figure 2.1 taken from [6], the difficulty of linearising the pressure loss, without considering the range of the fluid velocity, can be seen. It is the authors opinion that the effect of non-Newtonian drilling mud in the heave disturbance problem in MPD needs further investigation.

2.2 Well Model

The well model that will be presented here is based on the one presented in [23]. It incorporates appropriate changes due to the following properties of the MPD configuration :

- The well is sealed at the top.
- There is no flow through the BHA. Based on this we use the assumption that there is no flow in the fluid in the Drill String, and that the pressure in the drill string fluid

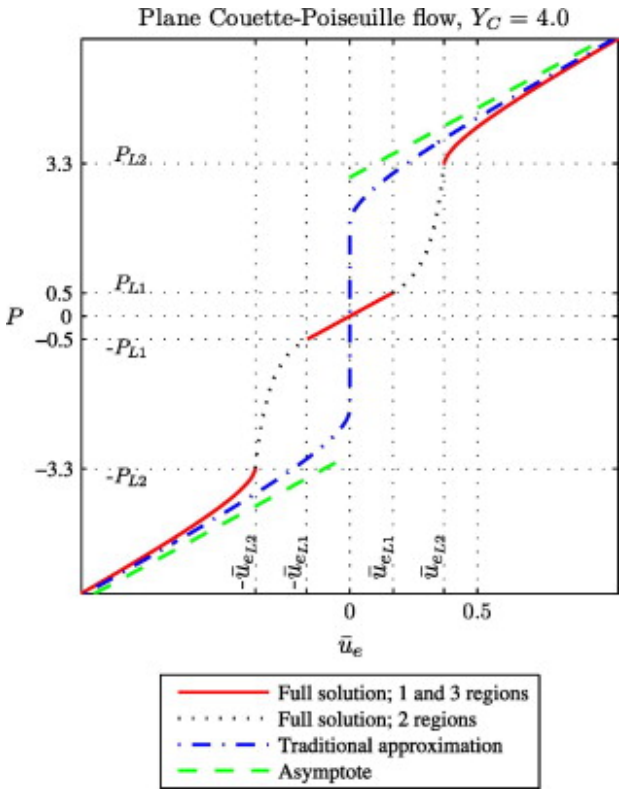

Figure 2.1: Dimensionless friction pressure gradient, P, vs dimensionless effective flow velocity, $\bar{u}_e$ for plane Couette-Poiseuille flow. $\bar{u}_e$ is a function of the mud average flow velocity and the drill string velocity. Figure is taken from [6].

is constant.

In deriving the governing equations of the well model we will use the following assumptions [11]:

- The flow is laminar, i.e., the Reynolds number is 2300 or less.
- The flow is axisymetrical. This assumption implies that the conduit is straight, although the equations works when the well have a relatively small radius of curvature.
- Motions in the radial direction is negligible. This implies that the longitudinal velocity component is much greater than the radial component and that pressure is constant across the cross section.
- Non-linear convective acceleration terms are negligible. This assumption is valid when the mud velocity is much smaller than the speed of sound in the mud.
- Material properties are constant.
- Thermodynamic effects are negligible.

The well model is divided into three sections (see Fig. 2.2), given by three sets of Partial differential equations: The 'Openhole Model', 'Annulus Model' and 'Elastic Drill String Model'. The PDEs describing the 'Annulus Model' and the 'Elastic Drill String Model' is coupled through the terms describing the viscous friction, and these two are again connected to the 'Openhole Model' through boundary conditions. Properties and functions related to the 'Openhole Model', 'Annulus Model' and 'Elastic Drill String Model' are denoted with the subscripts b, a and p respectively. Pressure and velocity p, v in the annulus and drill string are functions of time t and position x, where $x = 0$ is at the drill bit. Position in the openhole is denoted by x_b, where $x_b = 0$ is at the bottom of the openhole section and $x = L_b$ is at the top. p is defined as deviation from the steady state pressure, p^s at $t = 0$.

All the model sections are derived based on the one dimensional balance of mass and momentum [3]. For the one dimensional mass balance of a control volume of length dx we have that the change of mass in the control volume equals the flow inn minus the flow out of the volume

$$dx\frac{d\rho}{dt} = -\rho dv \tag{2.1}$$

Using the constitutive equation for a compressible mass with longitudinal[2] elasticity β: $dp = (\beta/\rho)d\rho$, gives

$$\frac{1}{\beta}\frac{dp}{dt} = -\frac{\partial v}{\partial x} \tag{2.2}$$

[2]Longitudinal elasticity because we are only interested in longitudinal waves (also known as compression waves).

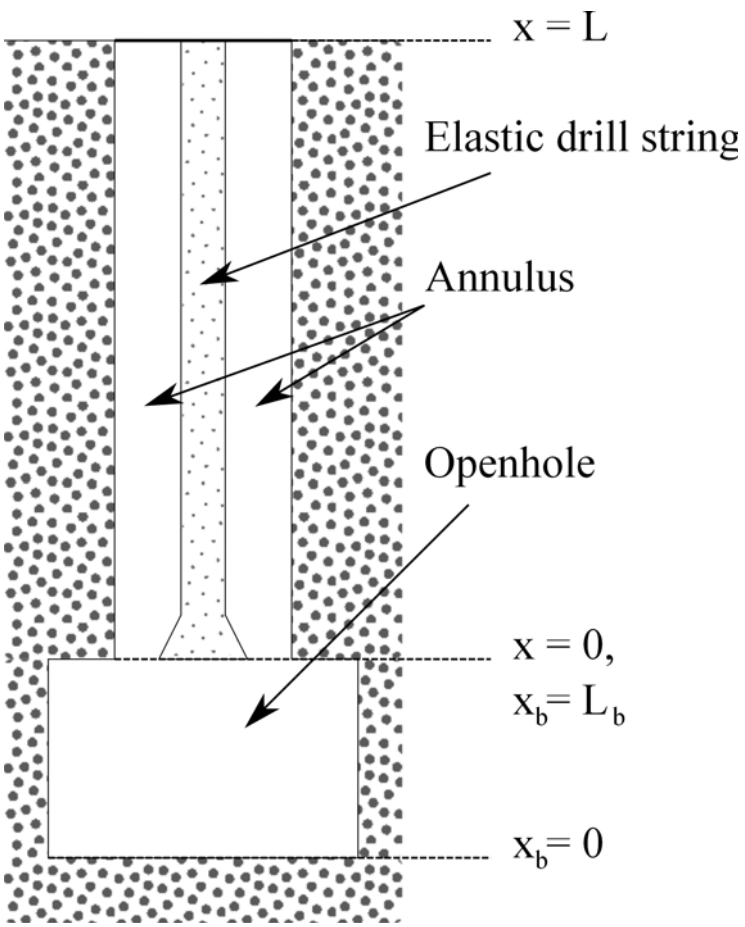

Figure 2.2: Schematic showing the three section of the well model.

For the one dimensional balance of momentum for the same control volume we have

$$\sum F = \frac{d}{dt}\rho v \; dx \tag{2.3}$$

Linearising the equation by using a constant mass density, ρ, and pulling out of the $\sum F$ term the pressure force acting on the sides of the control volume gives

$$\rho\frac{d}{dt}v = -\frac{\partial p}{\partial x} + F_a \tag{2.4}$$

where F_a are the forces acting on the mass in the control volume aside from the pressure. Together equations (2.2),(2.4) gives the unsteady pressure and velocity dynamics of an elastic medium.

2.2.1 Openhole Model

This is the section of the well that is below the BHA. The model is given by the balance of mass and momentum relations (2.2),(2.4)

$$\frac{1}{\bar{\beta}_b}\frac{dp_b}{dt} = -\frac{\partial v_b}{\partial x} \tag{2.5}$$

$$\rho\frac{\partial v_b}{\partial t} = -\frac{\partial p_b}{\partial x} - f_b(v_b) \tag{2.6}$$

Here $\bar{\beta}_b$ is the effective bulk modulus of the fluid in the borehole which takes into account the expansion of the hole caused by internal fluid pressure, dA/dp. $\bar{\beta}_b$ is derived in section 2.2.5. $f_b(v_b)$ is the drag on the fluid caused by viscous forces.

2.2.2 Annulus Model

Using mass and momentum balance

$$\frac{1}{\bar{\beta}_a}\frac{dp_a}{dt} = -\frac{\partial v_a}{\partial x} \tag{2.7}$$

$$\rho\frac{\partial v_a}{\partial t} = -\frac{\partial p_a}{\partial x} - f_a(v_a, v_p) \tag{2.8}$$

Note the inclusion of the pipe velocity v_p in the viscous friction term. This term will be discussed in section 2.2.6.

When the flow cross section area of the annulus A_a changes this is enforced by splitting up the model describing the annulus dynamics into two and connecting them through the boundary conditions. To do this we use the mass balance, using $+, -$ to denote upstream and downstream respectively (see Fig. 2.3)

$$A_a^+ v_a^+ = A_a^- v_a^- + \Delta A_p v_p \tag{2.9}$$

$$p_a^+ = p_a^- \tag{2.10}$$

where ΔA_p is the change in pipe cross section area. Pressures can be considered constant across the area changes if the irreversible pressure loss due to the area change is negligible.

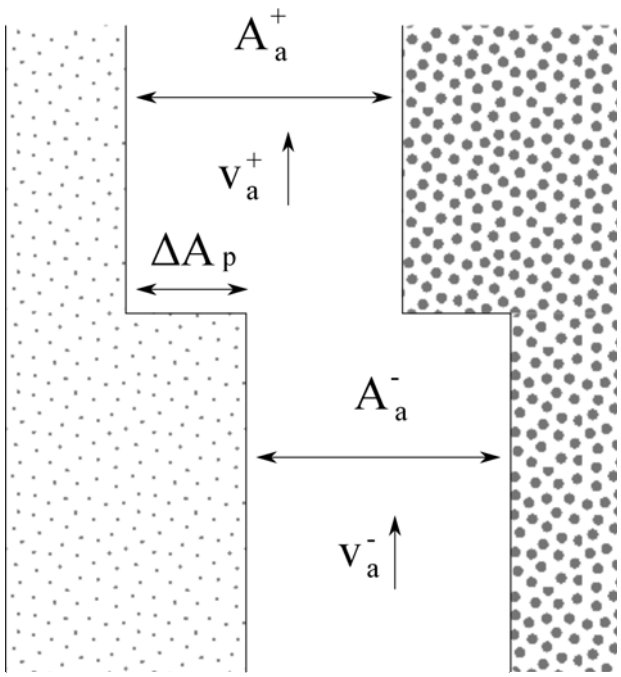

Figure 2.3: Schematic showing balance of mass for cross-sectional area changes.

2.2.3 Elastic Drill String

Again, using mass and momentum balance,

$$\frac{1}{\beta_p}\frac{dp_p}{dt} = -\frac{\partial v_p}{\partial x} \tag{2.11}$$

$$\rho_p \frac{\partial v_p}{\partial t} = -\frac{\partial p_p}{\partial x} + K_1 \frac{\partial}{\partial x} p_a - f_p(v_a, v_p) \tag{2.12}$$

Here β_p is the Youngs modulus of the pipe. The second term on the right side of equation 2.12 is due to the Hoop Stress effect. This is the effect of the pipe extending when being squeezed by high mud pressures. The last term is the viscous drag of the drill mud on the pipe.

2.2.4 Boundary Conditions

The topside boundary conditions

For the annulus we can choose either the topside pressure or the topside flow to be exogenous. I. e. only one of the following equations can be enforced

$p_a(x = L) = p_c,$	topside pressure in the annulus.
$A_a v_a(x = L) = q_{choke} - q_{bpp},$	flow through the choke and the back-pressure pump.

For the drill string we can choose either the force or the velocity at the top of the drill string to be exogenous. I.e. only one of the following equations can be enforced

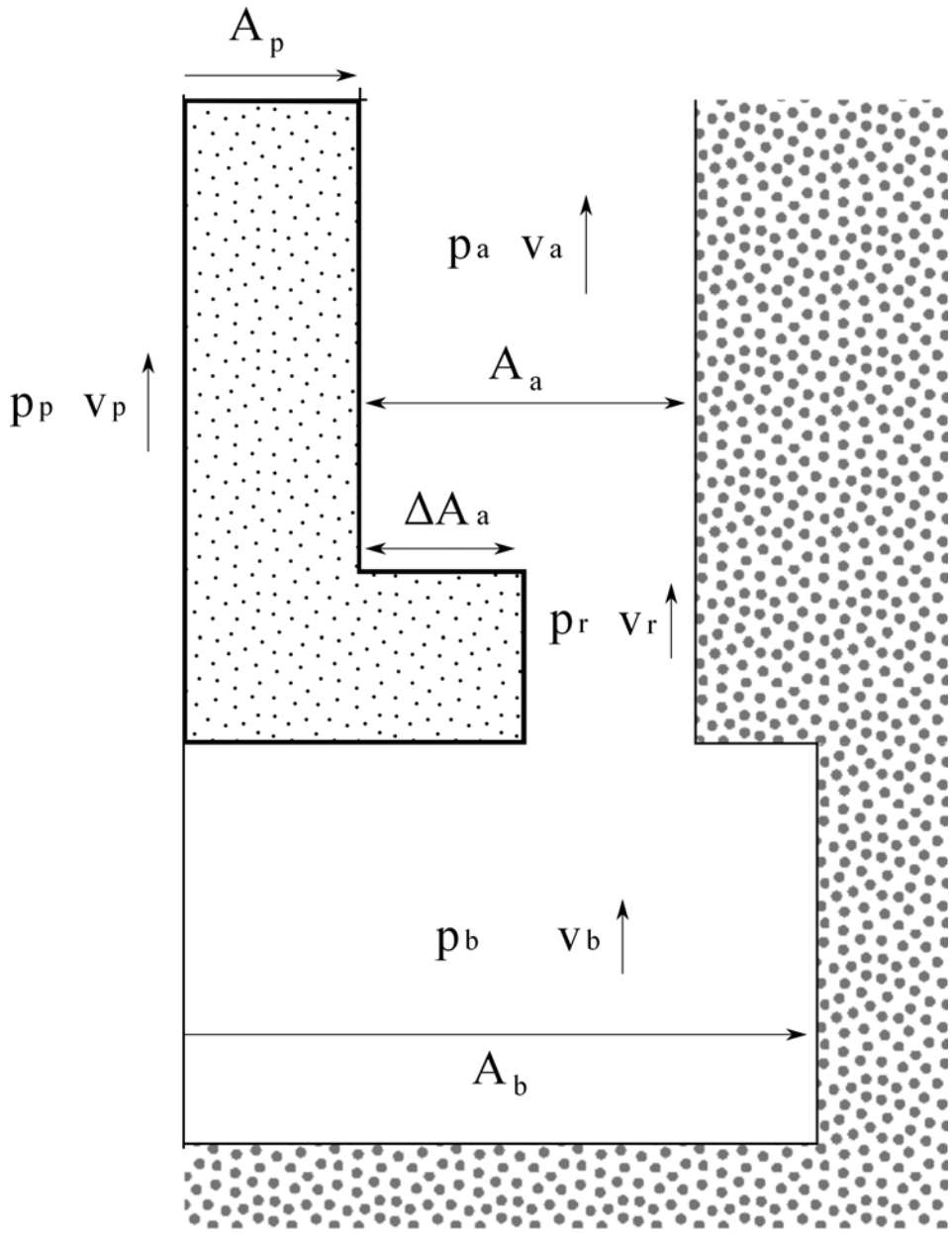

Figure 2.4: Schematic showing the coupling in the boundary conditions of the three model sections.

$v_p(x = L) = v_d$, topside movement of the pipe.
$A_p p_p(x = L) = F_d$, topside force on the pipe.

The bottomhole boundary conditions

Assuming rigid bottom-hole, $v_b(x_b = 0) = 0$ should be enforced.

Annulus to below drill string boundary condition

Letting ΔA_a be the change in the cross section area of the annulus around the drill bit, p_r be the pressure in the mud around the drill bit and v_r the velocity around the drill bit (see Fig. 2.4). Using mass balance

$$A_a v_a = (A_a - \Delta A_a)v_r + \Delta A_a v_p \tag{2.13}$$
$$A_b v_b = (A_a - \Delta A_a)v_r + (\Delta A_a + A_p)v_p \tag{2.14}$$

For the pressures, we use nozzle-pressure relations

$$p_r - p_b = \frac{\rho}{C_d}(v_b^2 - v_r^2) \tag{2.15}$$
$$p_a - p_r = \frac{\rho}{C_d}(v_r^2 - v_a^2) \tag{2.16}$$

Where C_d is the discharge coefficient. Note that the coefficient C_d is different for flow into a restriction and flow out of a restriction.

2.2.5 Borehole Expansion

The cross section area of the annulus is

$$A_a = \pi\Big((r_o + u_o)^2 - (r_i + u_i)^2\Big) \tag{2.17}$$

Where r_i, r_o is the inner and outer radius of the annulus, and u_i, u_o is the displacement of the inner and outer radius of the annulus. We want to find the displacement of the inner and outer annulus radius caused by the pressure in the annulus.

$$u_i = \frac{r_i}{E_i}(1 - \mu_i)p_a \tag{2.18}$$
$$u_o = -\frac{r_o}{E_o}(1 + \mu_o)p_a \tag{2.19}$$

where E_i, E_o and μ_i, μ_o is the Youngs modulus and Poissons ratio of the pipe and formation respectively. From these equations the relative expansion of the annulus cross section area can be determined (assuming that u_i, u_o is small compared to r_i, r_o):

$$\frac{1}{A_a}\frac{dA_a}{dP_a} = \frac{2r_o^2(1 + \mu_o)}{E_o(r_o^2 - r_i^2)} + \frac{2r_i^2(1 - \mu_i)}{E_i(r_o^2 - r_i^2)} \tag{2.20}$$

And the effective bulk modulus of the drilling mud in the annulus $\bar{\beta}_a$ becomes

$$\frac{1}{\bar{\beta}_a} := \left|\frac{2r_o^2(1+\mu_o)}{E_o(r_o^2-r_i^2)} + \frac{2r_i^2(1-\mu_i)}{E_i(r_o^2-r_i^2)} + \frac{1}{\beta}\right| \tag{2.21}$$

where β is the bulk modulus of the drilling mud.

For the openhole section the relation simplifies to

$$\frac{1}{\bar{\beta}_b} := \left|\frac{2(1+\mu_b)}{E_o} + \frac{1}{\beta}\right| \tag{2.22}$$

2.2.6 Viscous Friction

Calculating the viscous friction for a dynamic model becomes very involved for the case of non-Newtonian fluids (see Fig. 2.5). Depending on the pressure gradient, the velocity of the drill string and mud rheology, the velocity profile may have one, two or three flow regions for a Bingham Plastic [6], and the analytical solution for pressure loss w.r.t. velocity is implicit. An explicit approximation of the pressure gradient for a Bingham plastic is given in [6], and the analytical (and implicit) solution for unsteady flow in Power Law fluids are given in [25].

For the case of Newtonian drilling mud, the viscous friction becomes a linear function of the average velocity and drill string velocity. Using r_i, r_o to denote the inner and outer radius of the annulus. From [6] we have

$$f_a(v_a, v_p) = -12\frac{\mu}{(r_o-r_i)^2}v_a + 6\frac{\mu}{(r_o-r_i)^2}\alpha_1 v_p, \tag{2.23}$$

$$\alpha = \frac{r_i}{r_o}, \tag{2.24}$$

$$\alpha_1 = \frac{8\alpha^4\ln(\alpha)^2 + \alpha_4\alpha_5\ln(\alpha) + 2\alpha^2\alpha_5^2}{-\alpha_2\alpha_3\alpha_5}, \tag{2.25}$$

$$\alpha_2 = 2\ln(\alpha) + 1 - \alpha^2, \tag{2.26}$$

$$\alpha_3 = 2\alpha^2\ln(\alpha) + 1 - \alpha^2, \tag{2.27}$$

$$\alpha_4 = 3\alpha^4 + 6\alpha^2 - 1, \tag{2.28}$$

$$\alpha_5 = (1-\alpha)^2 \tag{2.29}$$

where μ is the viscosity of the fluid. Defining

$$k_a := 12\mu/(r_o-r_i)^2, \tag{2.30}$$

$$k_d := 6\mu\alpha_1/(r_o-r_i)^2, \tag{2.31}$$

$$k_p := \frac{A_p}{A_a}k_d, \tag{2.32}$$

$$k_b := \frac{4\mu\pi}{A_b} \tag{2.33}$$

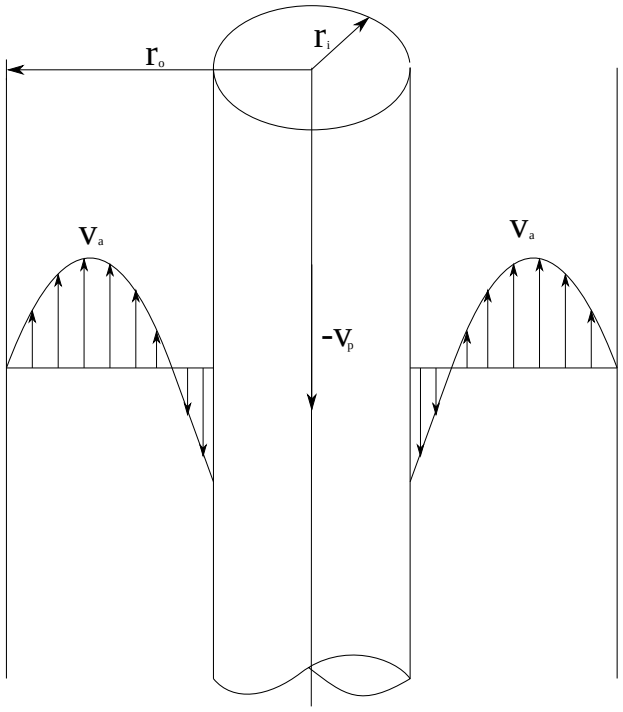

Figure 2.5: Schematic showing the velocity distribution of pressure driven couette flow in an annulus.

we obtain for Newtonian drilling muds

$$f_a(v_a, v_p) = k_a v_a - k_d v_p, \tag{2.34}$$
$$f_p(v_a, v_p) = k_p(v_p - v_a), \tag{2.35}$$
$$f_b(v_b) = k_b v_b \tag{2.36}$$

2.2.7 Implementation

In [23] the well model is implemented in simulations in the following way. The interpolated method of characteristics is used to solve the fluid-flow part of the coupled drill string/annulus model and the openhole model [2]. The elastic drill string motion is solved by use of finite elements to determine the equations which are solved by use of the tridiagonal algorithm [13]. For nonlinear boundary conditions, Newtons method is used.

2.3 Model Simplification

The well model derived in section 2.2 is complex with the model sections coupled by implicit relations in the boundary conditions, and for non-Newtonian fluids the flow equations also becomes implicit. Thus it is difficult to implement in simulations and controller design.

We will in the following discuss how the model can be simplified, under what assumptions these simplifications may hold as well as to what end they may be performed.

2.3.1 Explicit/Linear Model

To obtain a model where all relations are explicit, two simplifications must be made. The nozzle pressure relations must be discarded[3] and in the case of non-Newtonian fluid the viscous friction coupling the annulus flow and the drill string movement must be substituted with an explicit approximation, such as the one given in [6]. Obtaining an explicit model makes it easier to simulate and analyse for controller design.

To obtain a linear model, we need the same simplifications as above, with the addition that the explicit approximation of the viscous friction is linear w.r.t. both the drills string and annulus flow velocity. We note that this is true for laminar flow of a Newtonian drilling mud. Obtaining a linear model allows for superposition of the response of the system with regards to both time and inputs. This means that we can analyse the behaviour of the system by studying the impulse response from the different exogenous inputs since the response of a linear system is the convolution of the input signal with the impulse response. This again allows for frequency domain techniques to be employed.

The model can be discretized by approximating the hyperbolic PDEs by finite number of ODEs. This is done by letting the control volumes be of some finite, non-zero length. This allows for easier implementation in simulations and allows for using the theory of non-linear ODE systems for analysis and controller design. If the discretization is combined with a the linear approximation the resulting system becomes a a finite dimensional LTI system which allows for employing standard LTI control methods and frequency domain analysis.

2.3.2 Caveats of Model Simplification

When heave and surge models have been compared with data from field tests in the literature ([24], [23]) it have been found that effects which are negligible in some wells are dominating in others. Hence the author wish to stress that the simplification of the model given in section 2.2 should be done on a case by case basis and after due consideration of properties such as well geometry and mud rheology: A linear relation for the viscous friction will is correct for a Newtonian drilling mud, but not for a Bingham Plastic with high yield stress, etc..

[3]Discarded or substituted by an explicit relation but it may be difficult to obtain a bidirectional explicit relation of a set of nozzle equations.

2.4 Implementation a of Finite Dimensional LTI Well Model

We will now describe how a finite dimensional LTI approximation of the model can be implemented.

2.4.1 Linear distributed system

We will use the simplifications discussed above; assuming a Newtonian drilling mud and ignoring the implicit nozzle pressure relations so that we obtain a linear model. For the viscous friction we will use the relations found in 2.2.6. The governing equations becomes

$$\frac{dp_a}{dt} + \bar{\beta}_a \frac{\partial v_a}{\partial x} = 0 \tag{2.37}$$

$$\rho \frac{\partial v_a}{\partial t} + \frac{\partial p_a}{\partial x} + k_a v_a - k_d v_p = 0 \tag{2.38}$$

$$\frac{dp_b}{dt} + \bar{\beta}_b \frac{\partial v_b}{\partial x} = 0 \tag{2.39}$$

$$\rho \frac{\partial v_b}{\partial t} + \frac{\partial p_b}{\partial x} + k_b v_b = 0 \tag{2.40}$$

$$\frac{dp_p}{dt} + \rho_p \frac{\partial v_p}{\partial x} = 0 \tag{2.41}$$

$$\rho \frac{\partial v_p}{\partial t} + \frac{\partial p_p}{\partial x} + k_p(v_p - v_a) + K_1 \frac{\partial}{\partial x} p_a = 0 \tag{2.42}$$

These equations have a total of six integrations which means six boundary conditions have to be specified. Recall that the nozzle pressure relations have been ignored to achieve linearity.

$$A_a v_a(x = L) = q_c - q_{bpp} \tag{2.43}$$

$$p_a(x = 0) = p_b(x_b = L_b) \tag{2.44}$$

$$v_p(x = L) = v_d \tag{2.45}$$

$$p_p(x = 0) = p_b(x_b = L_b) + p_b^s(x_b = L_b) \tag{2.46}$$

$$A_b v_b(x_b = L_b) = A_a v_a(x = 0) + A_p v_p(x = 0) \tag{2.47}$$

$$v_b(x = 0) = 0 \tag{2.48}$$

where q_c, q_{bpp}, v_d are exogenous inputs to the system, and p_b^s is the steady state pressure at $t = 0$ which again equals the hydrostatic pressure plus the steady state pressure at the choke at $t = 0$.

If there are changes in the flow-area in any of the three sections, the section has to be split up and appropriate boundary conditions between the two resulting parts enforced as discussed in section 2.2.2.

2.4.2 Discretization

We use N control volumes to describe the dynamics in the annulus and the drill string. To maximize performance for a given order of the system the annulus should use more control volumes than the drill string because of the lower wave speed in the annulus, but it is much easier to describe the coupling in the viscous friction when the number of control volumes are the same. We use N_b control volumes to describe the dynamics in the borehole below the drill string. Define volume 1 to be at the bottom of the section and volume N, N_b to be at the top. The lengths of the sections are $\sum_{j=1}^{N} l_j$ and $\sum_{j=1}^{N_b} l_b^j$ for the annulus/drill-string and drill string to bottom-hole section respectively. The dynamic order of the resulting system is $4N + 2N_b$.

$$\dot{p}_a^j = \frac{\bar{\beta}_a^j}{l_j}(v_a^{j-1} - v_j), \qquad j = 1, \ldots, N \tag{2.49}$$

$$\rho \dot{v}_a^j = \frac{1}{l^j}(p_a^j - p_a^{j+1}) - k_a^j v_a^j + k_d^j v_p^j, \qquad j = 0, \ldots, N-1 \tag{2.50}$$

$$A_a^N v_N = q_c, \quad p_a^0 = p_b^{N_b}, \tag{2.51}$$

$$\dot{p}_p^j = \frac{\rho_p^j}{l^j}(v_p^{j-1} - v_p^j), \qquad j = 1, \ldots, N \tag{2.52}$$

$$\rho_p \dot{v}_p^j = \frac{1}{l^j}(p_p^j - p_p^{j+1}) - k_p^j(v_p^j - v_a^j) + \frac{K_1}{l^j}(p_a^j - p_a^{j+1}), \qquad j = 0, \ldots, N-1 \tag{2.53}$$

$$v_p^N = v_d, \quad p_p^0 = p_b^{N_b}, \tag{2.54}$$

$$\dot{p}_b^j = \frac{\bar{\rho}_b}{l_b^j}(v_b^{j-1} - v_b), \qquad j = 1, \ldots, N_b \tag{2.55}$$

$$\rho \dot{v}_b^j = \frac{1}{l_b^j}(p_b^j - p_b^{j+1}) + k_b^j v_b^j, \qquad j = 0, \ldots, N_b - 1 \tag{2.56}$$

$$v_b^0 = 0, \quad A_b v_b^{N_b} = A_a v_a^0 + A_p v_p^0 \tag{2.57}$$

when there is a change in the cross sectional flow area of the annulus, the equations should be modified. For a change in the cross sectional area between control volume j and $j-1$, the modification is as follows (see Fig. 2.6)

$$\dot{p}_a^j = \frac{1}{A_a^j}(A_a^{j-1} v_a^{j-1} + \Delta A_p v_p^{j-1}) - v_a^j \tag{2.58}$$

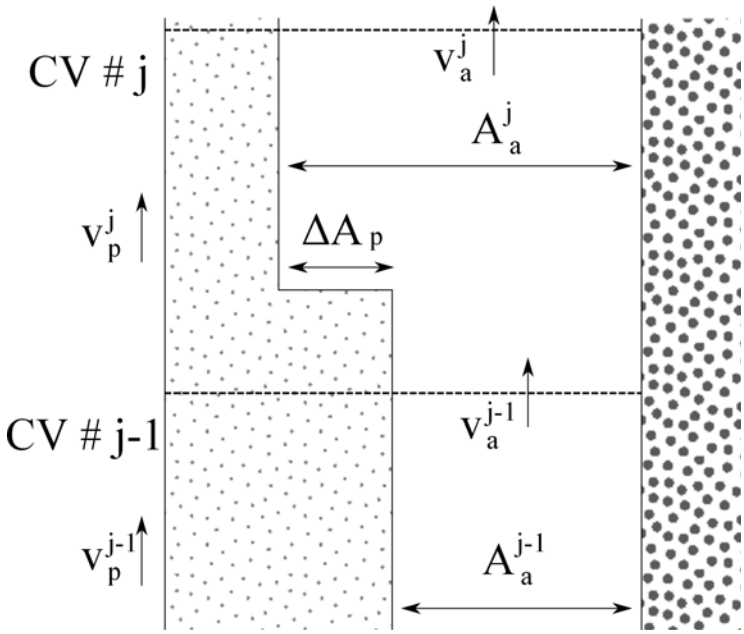

Figure 2.6: Schematic showing the balance of mass for cross sectional-area changes in the discretized model.

Chapter 3

Analysis of Simplified Model

Analysis of the simplified model and the error introduced by the discretization of the model. To keep this chapter as clear as possible, the drill string to bottom-hole section of the model is not included in this analysis, i.e. the drill string is assumed to be close to the bottom of the well. Further it is assumed that the drill string is inelastic, i.e. $v_p = v_d,\ \forall x$. The reason for this assumption is that if v_p is dependent on x then finding the particular solution of equation (3.8) becomes difficult.

Since we are only considering annulus dynamics in this simplified model, we will drop the a subscripts of the velocity, pressure and cross section area in the annulus, i.e. $v := v_a, p := p_a, A := A_a$.

3.1 Transfer Function of the Simplified Model

Writing the linear model of the annulus dynamics in distributed form

$$\frac{\partial p}{\partial t} = -\beta \frac{\partial v}{\partial x} \tag{3.1}$$

$$\frac{\partial v}{\partial t} = -\frac{1}{\rho}\frac{\partial p}{\partial x} - k_a v + k_d v_d + \tag{3.2}$$

As (3.1)-(3.2) is linear the constant term due to the gravitational force will not effect the dynamics of the system, only the steady state and so it has been discarded.

3.1.1 Laplace Transformed System

Using subscript notation to denote partial derivatives, (3.1)-(3.2) can be written as

$$p_t + \beta v_x = 0 \tag{3.3}$$

$$v_t + \frac{A}{\rho_0} p_x + k_a v - k_d v_d = 0 \tag{3.4}$$

Differentiating (3.3) w.r.t. to x and (3.4) w.r.t. t;

$$p_{tx} + \beta v_{xx} = 0 \tag{3.5}$$

$$v_{tt} + \frac{1}{\rho} p_{xt} + k_a v_t - k_d \dot{v}_d = 0 \tag{3.6}$$

Inserting (3.5) for p_{xt} in (3.6). This gives

$$v_{tt} - c^2 v_{xx} + k_a v_t = k_d \dot{v}_d, \quad c = \sqrt{\frac{\beta}{\rho_0}} \tag{3.7}$$

This is the one dimensional wave equation with dissipation driven by the heave motion, and c is the speed of sound. By utilizing the Laplace transform we want to derive the transfer function of the system. Taking the Laplace transform of (3.7), denoting the Laplace transformed functions by $\hat{v}, \hat{p}$, and assuming steady-state at $t = 0$ (i.e. that $v(x, 0) = 0$), we get

$$\hat{v}_{xx} - \hat{v} \frac{1}{c^2}(s^2 + s k_a) = -\frac{k_d}{c^2} s \hat{v}_d \tag{3.8}$$

This is a inhomogeneous second order Ordinary Differential Equation in x and can be solved for $\hat{v}(x, s)$. Defining $\gamma^2 := \frac{1}{c^2}(s^2 + sk)$, the homogeneous solution is

$$\hat{v}_h(x, s) = \ C_1 \sinh(\gamma x) + \ C_2 \cosh(\gamma x) \tag{3.9}$$

where C_1, C_2, are integration constants that have to be solved from the boundary conditions. The particular solution is

$$\hat{y}_p = \frac{k_d}{\gamma^2 c^2} s v_d = \frac{k_d}{s + k_a} \hat{v}_d \tag{3.10}$$

The general solution is

$$\hat{v}(x, s) = \ C_1 \sinh(\gamma x) + \ C_2 \cosh(\gamma x) + \hat{y}_p \tag{3.11}$$

3.1.2 Solving for Boundary Conditions

The boundary conditions are the flow into the bottom of the well, and flow out of the top of the well. Assuming that the movement of the drilling bit can be modelled as a volumetric flow into the bottom of the well, we have $A\hat{v}(0, s) = A_d \hat{v}_d(s)$, where A_d is the cross section area of the drilling bit. Denoting the flow through the choke at the top of the well by q_c,

we have $A\hat{v}(L,s) = \hat{q}_c(s)$. Enforcing these boundary conditions on (3.11), we get

$$\hat{v}(x=0,s) = C_2 + \hat{y}_p = \frac{A_d}{A}\hat{v}_d(s) \tag{3.12}$$

$$\implies C_2 = \frac{A_d}{A}\hat{v}_d - \hat{y}_p \tag{3.13}$$

$$\hat{v}(x=L,s) = C_1\sinh(\gamma L) + C_2\cosh(\gamma L) + \hat{y}_p = \frac{\hat{q}_c}{A} \tag{3.14}$$

$$\implies C_1 = \frac{\hat{q}_c}{A}\frac{1}{\sinh(\gamma L)} - C_2\frac{\cosh(\gamma L)}{\sinh(\gamma L)} - \frac{\hat{y}_p}{\sinh(\gamma L)} \tag{3.15}$$

$$= \frac{\hat{q}_c}{A}\frac{1}{\sinh(\gamma L)} - \frac{A_d}{A_a}\hat{v}_d\frac{\cosh(\gamma L)}{\sinh(\gamma L)} \tag{3.16}$$

$$+ \hat{y}_p\Big(\frac{\cosh(\gamma L)}{\sinh(\gamma L)} - \frac{1}{\sinh(\gamma L)}\Big) \tag{3.17}$$

Substituting C_1 and C_2 into (3.11) we get

$$\hat{v}(x,s) = \hat{v}_c(s)\frac{\sinh(\gamma x)}{\sinh(\gamma L)} \tag{3.18}$$

$$+ \frac{A_d}{A}\hat{v}_d\Big(\cosh(\gamma x) - \frac{\sinh(\gamma x)}{\tanh(\gamma L)}\Big) \tag{3.19}$$

$$+ \hat{y}_p\Big(\frac{\sinh(\gamma x)}{\tanh(\gamma L)} - \frac{\sinh(\gamma x)}{\sinh(\gamma L)} - \cosh(\gamma x) + 1\Big) \tag{3.20}$$

Differentiating with respect to x, we get

$$\hat{v}_x(x,s) = \hat{q}_c(s)\frac{\gamma}{A}\frac{\cosh(\gamma x)}{\sinh(\gamma L)} \tag{3.21}$$

$$+ \frac{A_d}{A}\hat{v}_d\gamma\Big(\sinh(\gamma x) - \frac{\cosh(\gamma x)}{\tanh(\gamma L)}\Big) \tag{3.22}$$

$$+ \hat{y}_p\gamma\Big(\frac{\cosh(\gamma x)}{\tanh(\gamma L)} - \frac{\cosh(\gamma x)}{\sinh(\gamma L)} - \sinh(\gamma x)\Big) \tag{3.23}$$

and inserting into the Laplace transform of (3.3), we obtain

$$\hat{p}(x,s) = -\frac{\beta}{s}\hat{v}_x(x,s) \tag{3.24}$$

where $p(x,0) = 0$ assuming the well dynamics are at steady state at $t = 0$ (i.e. $p(x,t) = 0$). (3.24) can be solved for $p(x=0,s)$ and $p(x=L,s)$ to obtain p_{bit} and p_c respectively, and because the system is linear the inputs v_d, q_c can be considered separately. We can write the well model as a system with inputs v_d, q_c and outputs p_{bit}, p_c

$$\begin{bmatrix} p_{bit} \\ p_c \end{bmatrix} = P \begin{bmatrix} v_d \\ q_c \end{bmatrix} \tag{3.25}$$

where P is a two by two transfer function matrix

$$P = \begin{bmatrix} P_{11} & P_{12} \\ P_{21} & P_{22} \end{bmatrix} \tag{3.26}$$

3.1.3 Mud Clinging Effect vs Mud Displacement Effect

We see from the solution of the Laplace-transformed linearised system that the effects affecting pressure distribution of the well can be decomposed into three parts. The three effects are due to the flow into the top of the annulus, the mud displacement of the drill string moving into the annulus and mud clinging to the moving drill string, given by the equations (3.21), (3.22) and (3.23) respectively. These equations evaluated along $s = i\omega$ is shown in Fig. 3.1 for the physical properties given in table 3.1, and shows the magnitude of the effects for different input frequencies. It can be seen that the mud clinging effect relative to the other two effects increases with increased mud viscosity and well length. We denote the frequency of the first resonance peak as $\omega_{r,1}$. It can be seen that when the mud viscosity is $88cP$ the mud clinging effect has a higher magnitude than the other effects for frequencies over $\omega_{r,1}/4$. For a mud viscosity of $12cP$ (and lower) the mud clinging effect will not be significant when the input frequency are less than $\omega_{r,1}/2$.

We also note that the resonance frequencies occur at lower frequencies when the length of the well is increased.

3.2 Comparison with the Discretized System

As the PDE is hyperbolic, information travels with a finite velocity given by the speed of sound in the mud. To maintain this property a large number of Control Volumes may be needed in the discretization.

In the following, a typical drilling well is considered, again with the physical properties shown in Table 3.1. The frequency response of P_{11} is plotted in In Fig. 3.2 and Fig. 3.3 together with the discretized version. The frequency response of P_{21} is shown in appendix A.1. In Fig. 3.2 and Fig. 3.3 it can be seen how the discretization based on 2 control volumes quickly deteriorates in accuracy as frequency increases. The 50 control volumes discretization shows that high accuracy can be achieved at the cost of increased model complexity. We also note that when the length of the well increases accuracy deteriorates as the length of each control volume increases.

3.2.1 Resonance Frequencies

The irrational transfer functions in the transfer function matrix P defined in (3.25) have damped resonance peaks at their Resonance frequencies which occurs when $\sinh(\gamma L)$ is zero. Using the approximation

$$\frac{L}{c}\sqrt{-\omega^2 + k_a\omega i} \approx \frac{L}{c}\Big(\omega i + \frac{k_a}{2}\Big) \tag{3.27}$$

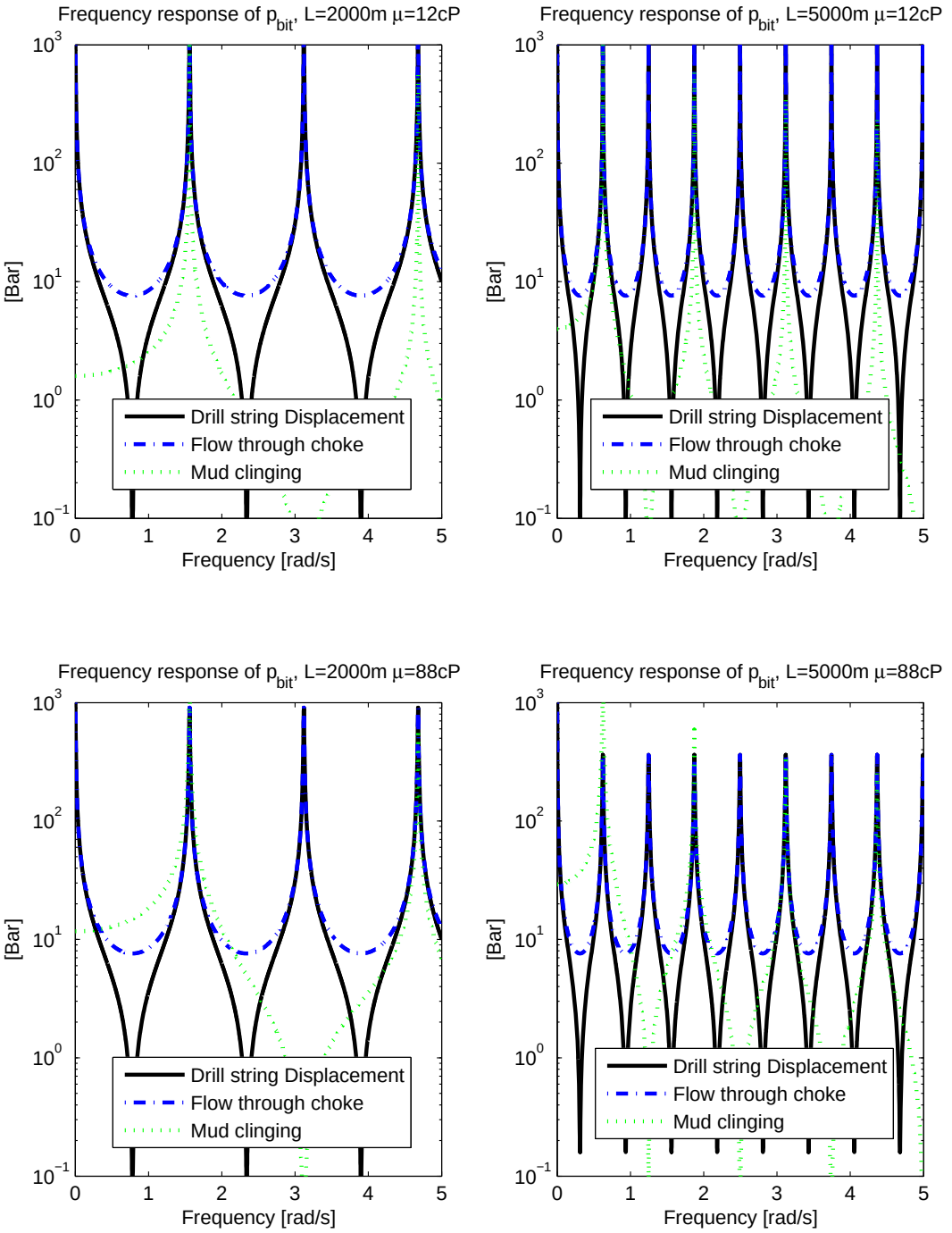

Figure 3.1: Comparison of the 3 effects affecting the down-hole pressure for different well lengths and mud viscosities.

Table 3.1: The physical properties of the well

Parameter	**Value**
Length of well L	$2000, 5000[m]$
Annulus outer radius r_o	$0.113[m]$
Annulus inner radius r_i	$0.0635[m]$
Cross section area of drilling bit A_d	$0.0148[m^2]$
Effective Bulk Modulus $\bar{\beta}_a$	$1.4 * 10^9[Pa]$
Drilling Mud Mass Density ρ	$1420[kg/m^3]$
Mud Viscosity μ	$12, 88[cP]$

which is valid when ω is not close to 0, we can write

$$\sinh\Big(\frac{L}{c}\Big(\omega i + \frac{k_a}{2}\Big)\Big) = \tag{3.28}$$

$$\sinh\Big(\frac{Lk}{2c}\Big)\cos\Big(\frac{L\omega}{c}\Big) + i\cosh\Big(\frac{Lk}{2c}\Big)\sin\Big(\frac{L\omega}{c}\Big) \tag{3.29}$$

It can be seen that the damped resonance frequencies occurs at $\omega_{r,j} = \frac{j\pi c}{l},\ j = 1, 2, \ldots,$ and that as $\frac{Lk}{c}$ becomes larger the resonance decreases in magnitude.

For comparison, the resonance frequencies of the discretized system can be found by calculating the eigenvalues of the system matrix. The system matrix has an eigenvalue in 0 and $N-1$ pairs of complex conjugated eigenvalues with real part $-\frac{k_a}{2}$ and complex part equal the resonance frequency in rad/s of the corresponding damped resonance peak. The resonance frequencies of the discretized systems of 2 to 5 control volumes can be found in Table 3.2. We note that the accuracy of the discretization increases significantly when increasing the number of control volumes also for low frequencies. This is also seen in Fig. 3.2 and Fig. 3.3.

Table 3.2: Resonance Frequencies evaluated for the Properties given in Table 3.1 with $L = 2000m$

	$\omega_{r,1}$	$\omega_{r,2}$	$\omega_{r,3}$	$\omega_{r,4}$
P	$\frac{\pi}{L}\sqrt{\frac{\beta}{\rho_0}} = 1.56$	$2\frac{\pi}{L}\sqrt{\frac{\beta}{\rho_0}} = 3.12$	$3\frac{\pi}{L}\sqrt{\frac{\beta}{\rho_0}} = 4.68$	$4\frac{\pi}{L}\sqrt{\frac{\beta}{\rho_0}} = 6.24$
$\tilde{P}^2$	$2\frac{\sqrt{\frac{8\beta}{\rho_0}-\frac{k_a^2L^2}{2^2}}}{2L} = 1.40$			
$\tilde{P}^3$	$3\frac{\sqrt{\frac{4\beta}{\rho_0}-\frac{k_a^2L^2}{3^2}}}{2L} = 1.49$	$3\frac{\sqrt{\frac{12\beta}{\rho_0}-\frac{k_a^2L^2}{3^2}}}{2L} = 2.58$		
$\tilde{P}^4$	$4\frac{\sqrt{\frac{4(2-\sqrt{2})\beta}{\rho_0}-\frac{k_a^2L^2}{4^2}}}{2L} = 1.52$	$4\frac{\sqrt{\frac{8\beta}{\rho_0}-\frac{k_a^2L^2}{4^2}}}{2L} = 2.81$	$4\frac{\sqrt{\frac{4(2+\sqrt{2})\beta}{\rho_0}-\frac{k_a^2L^2}{4^2}}}{2L} = 3.67$	
$\tilde{P}^5$	$5\frac{\sqrt{\frac{2(3-\sqrt{5})\beta}{\rho_0}-\frac{k_a^2L^2}{5^2}}}{2L} = 1.53$	$5\frac{\sqrt{\frac{2(5-\sqrt{5})\beta}{\rho_0}-\frac{k_a^2L^2}{5^2}}}{2L} = 2.92$	$5\frac{\sqrt{\frac{2(3+\sqrt{5})\beta}{\rho_0}-\frac{k_a^2L^2}{5^2}}}{2L} = 4.02$	$5\frac{\sqrt{\frac{2(5+\sqrt{5})\beta}{\rho_0}-\frac{k_a^2L^2}{5^2}}}{2L} = 4.72$

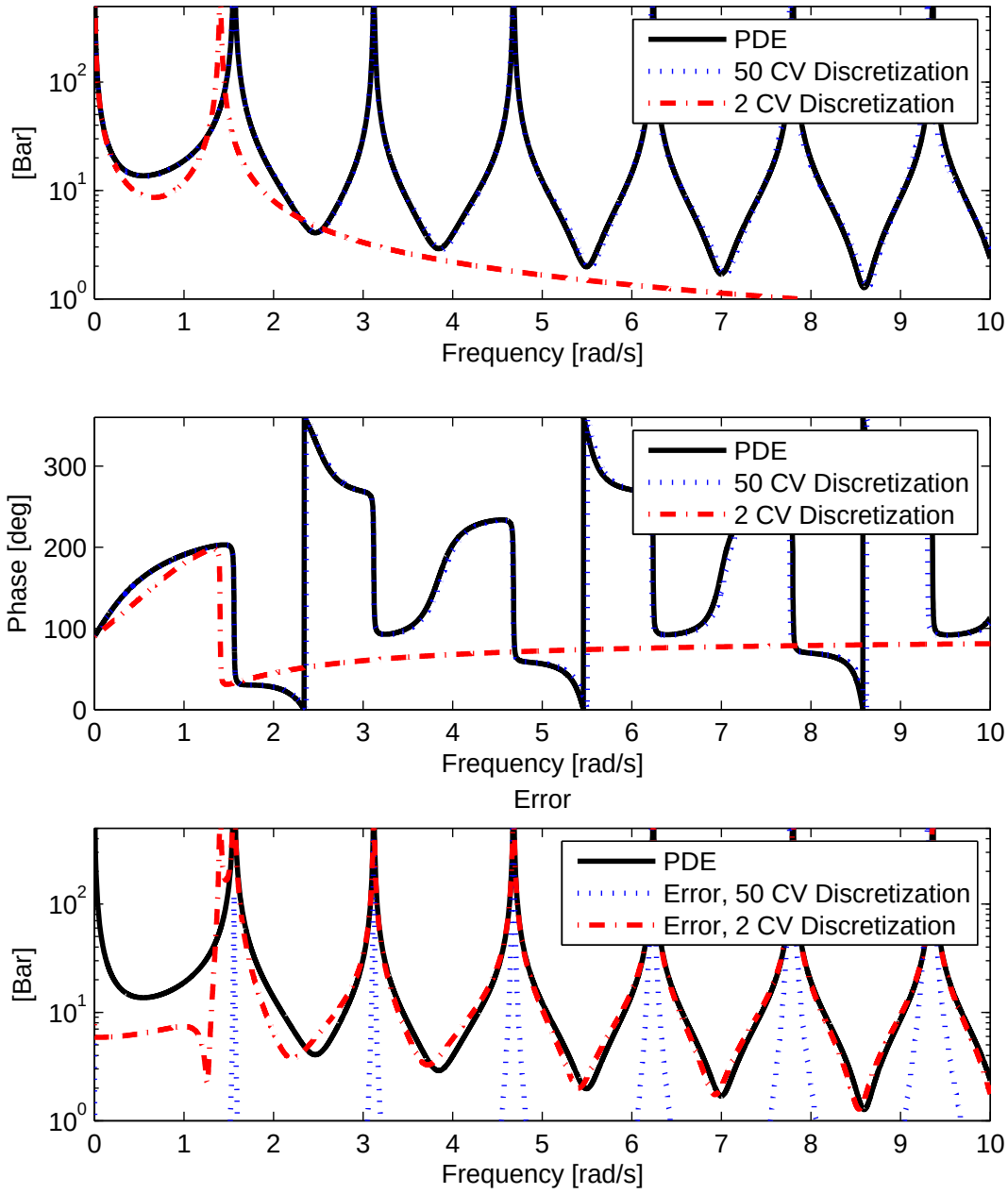

Figure 3.2: Gain and phase of the irrational transfer function P_{11} evaluated on the imaginary axis compared with transfer function of the discretized version of the same PDE with 2 and 50 Control Volumes Respectively. The length of well is 2000 meters.

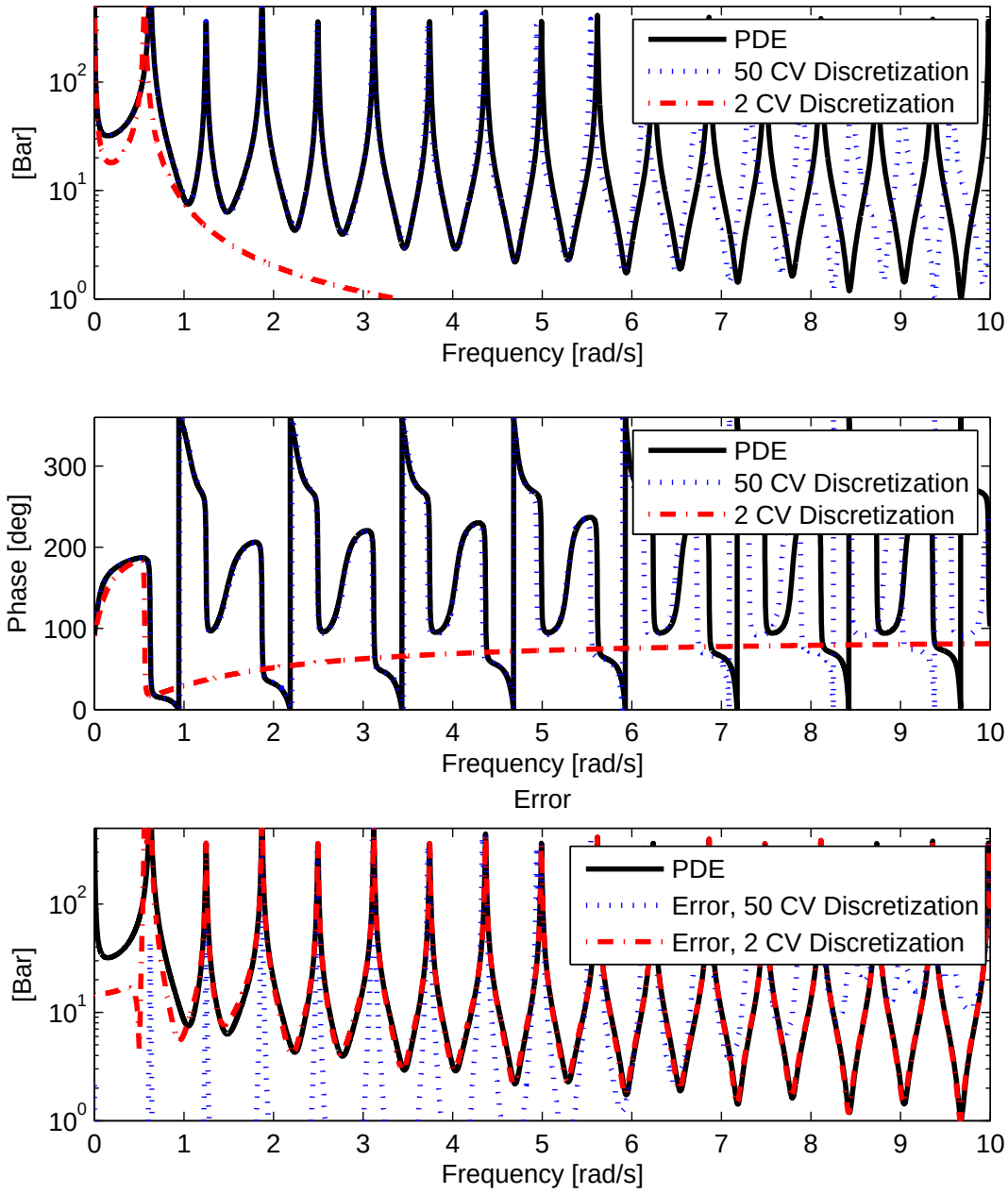

Figure 3.3: Gain and phase of the irrational transfer function P_{11} evaluated on the imaginary axis compared with transfer function of the discretized version of the same PDE with 2 and 50 Control Volumes Respectively. The length of the well is 5000 meters.

Chapter 4

Estimator Design

4.1 Implementation

4.1.1 State Space Configuration

Now we consider the task of designing an observer for the down-hole pressure. We will utilize measurements of the choke flow q_c, heave disturbance v_d and topside pressure p_c. As inputs we consider the choke flow and heave disturbance as frequency weighted disturbances with the frequency weight W_d, and white measurement noise.

$$\dot{x} = Ax + B_1 w(t), \quad x(0) = 0 \tag{4.1}$$

$$z = C_1 x \tag{4.2}$$

$$y = C_2 x + D_{11} w(t) + v(t) \tag{4.3}$$

$$\tilde{w} = \begin{bmatrix} v_d \\ q_c \end{bmatrix}, \quad v = \begin{bmatrix} v_1 \\ v_2 \\ v_3 \end{bmatrix}, \quad y = \begin{bmatrix} v_d + v_1 \\ q_c + v_2 \\ p_c + v_3 \end{bmatrix}, \quad z = p_{bit}, \quad w = W_d \tilde{w} \tag{4.4}$$

4.1.2 Input Weighting

As frequency weight for the disturbance input we use a function W_d fitted to the empirical frequency spectrum of floater heave as can be seen in Fig. 4.1.

$$W_d = \frac{0.12(s - 0.01)}{(s^2 - 0.02s + 0.0251)(s - 1)} \tag{4.5}$$

For the measurement noise standard deviation we use the values in table 4.1.2 which are typical in a MPD system.

4.1.3 Kalman Filter Design

Let a $2N - 1$th order discretization, made using N control volumes, of the of model be denoted $\tilde{P}^N$, and the $2N + 5$th order Kalman filter designed with this model be denoted

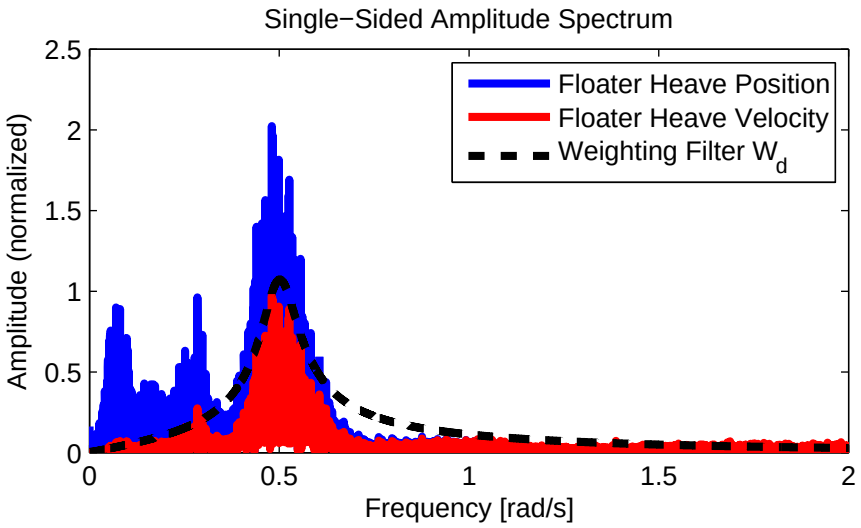

Figure 4.1: Empirical heave amplitude spectrum of disturbance.

Measurement	**Noise Standard Deviation**
Heave disturbance: v_1	0.1 [m]
Choke flow: v_2	50 [liter/min]
Topside Pressure: v_3	0.1 [Bar]
Disturbance	**Standard Deviation**
v_d	$1[m/s]$
q_c	888[liter/min]

Table 4.1: Standard deviation of noise and disturbance in the Kalman filter design.

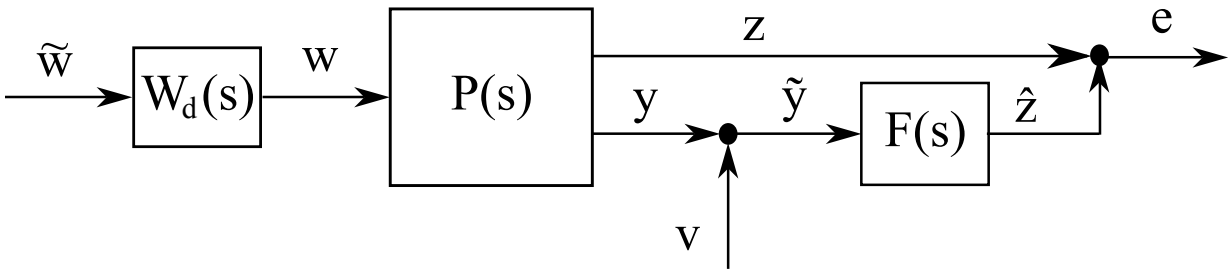

Figure 4.2: Kalman filter with weighted disturbance block diagram.

F^N (six states are added because of the weighting filter). Note that $F^N \in \mathcal{R}^{1\times 3}$ as it maps the three measurements to the estimate of downhole pressure, i.e.

$$\hat{z} := \hat{p}_{bit} = F^N y \tag{4.6}$$

The error dynamics becomes

$$e = z - \hat{z} = \left[\begin{array}{c} [P_{11}\ P_{12}] - F^N \left[\begin{array}{cc} 1 & 0 \\ 0 & 1 \\ P_{21} & P_{22} \end{array} \right], \quad F^N \end{array} \right] \left[\begin{array}{c} w \\ v \end{array} \right] \tag{4.7}$$

$$:= T^N_{ew,v} \left[\begin{array}{c} w \\ v \end{array} \right] \tag{4.8}$$

4.1.4 Computing Performance

As a performance measure, J, we use the standard deviation of the estimation error. We can compute the standard deviation of the estimation error by using the following relation [15]

$$J^j := \lim_{t\to\infty} E\Big(p^2_{bit}(t)\Big) \tag{4.9}$$

$$= \sqrt{\frac{1}{2\pi} \int_{-\infty}^{\infty} \text{Trace}\{T^{*j}_{ew,v}(i\omega) M T^{j}_{ew,v}(i\omega)\} d\omega}, \tag{4.10}$$

$$M := \left[\begin{array}{cc} Q & S' \\ S & R \end{array} \right], \tag{4.11}$$

$$Q := E(\tilde{w}\tilde{w}'), \quad R := E(vv'), \quad S := E(\tilde{w}v') \tag{4.12}$$

4.2 Obtaining Low Order Kalman Filters

There are three ways of obtaining a lower order filter. They are: First do model reduction and then filter design, first design the filter and then reduce it, and a direct low order design.

The reduce first approach is generally considered inferior to the design first approach [19], and is in particular not well suited in this case because the nominal plant is not strictly stable, hence it first has to be decomposed into its stable and unstable part before performing model reduction. This affects the weighting of the modes of the system and yields bad results which can be seen in appendix A.3. Hence we will here use the design first model reduction approach.

4.2.1 Balanced Model Reduction

This and the following section on Model Reduction is based on [15] and [22].

Suppose $G = \left[\begin{array}{c|c} A & B \\ \hline C & D \end{array}\right]$ is a stable and minimal realization of a system with controllability Gramian Σ_c and observability Gramian Σ_o, i.e.

$$\Sigma_c = \frac{1}{2\pi} \int_{-\infty}^{\infty} T_{xu}(i\omega) T_{xu}(i\omega)^* d\omega, \tag{4.13}$$

$$\Sigma_o = \frac{1}{2\pi} \int_{-\infty}^{\infty} T_{yx_0}(i\omega)^* T_{yx_0}(i\omega) d\omega, \tag{4.14}$$

$$T_{xu} := (sI - A)^{-1} B, \quad T_{yx_0} := C(sI - A)^{-1} \tag{4.15}$$

Note that for there to be a finite solution of 4.13 – 4.14 the system matrix must be strictly stable. There exists a balancing transformation T and a realization $\breve{G}$ such that

$$\breve{G} := \left[\begin{array}{c|c} \breve{A} & \breve{B} \\ \hline \breve{C} & \breve{D} \end{array}\right] := \left[\begin{array}{c|c} TAT^{-1} & TB \\ \hline CT^{-1} & D \end{array}\right] \tag{4.16}$$

yielding equal and diagonal Grammians $T\Sigma_c T^* = T^{-*}\Sigma_o T^{-1} \equiv \Sigma = \mathrm{diag}(\sigma_1, \sigma_2, \ldots, \sigma_n)$. Then $\breve{G}$ is called a balanced realization of G, and $\sigma_1, \sigma_2, \ldots, \sigma_n$ are the Hankel singular values of the system.

Assume that the Hankel singular values of the system is decreasingly ordered so that $\Sigma = \mathrm{diag}(\sigma_1, \sigma_2, \ldots, \sigma_n)$, and $\sigma_1 \geq \sigma_2 \geq \cdots \geq \sigma_n$. The states corresponding to the small singular values are less controllable and observable than the states corresponding to the larger singular values. Therefore, truncating those less controllable and observable states will yield less information loss than truncating other states.

Now partition the balanced Grammians as $\Sigma = \left(\begin{smallmatrix} \Sigma_1 & 0 \\ 0 & \Sigma_2 \end{smallmatrix}\right)$ where $\Sigma_1 = \mathrm{diag}(\sigma_1, \sigma_2, \ldots, \sigma_r)$, and $\Sigma_2 = \mathrm{diag}(\sigma_{r+1}, \sigma_{r+2}, \ldots, \sigma_n)$ and partition the system accordingly as

$$\breve{G} = \left[\begin{array}{cc|c} \breve{A}_{11} & \breve{A}_{12} & \breve{B}_1 \\ \breve{A}_{21} & \breve{A}_{22} & \breve{B}_2 \\ \hline \breve{C}_1 & \breve{C}_2 & \breve{D} \end{array}\right] \tag{4.17}$$

Then a reduced order system is the truncated system G_r

$$\breve{G}_r(s) = \left[\begin{array}{c|c} \breve{A}_{11} & \breve{B}_1 \\ \hline \breve{C}_1 & \breve{D} \end{array}\right] \tag{4.18}$$

And it can be shown that the truncated system is balanced and asymptotically stable [15].

4.2.2 Frequency Weighted Balanced Model Reduction

Let $y(s) = W_o(s)G(s)W_i(s)$, with W_i and W_o as input and output weights. The transfer function matrices becomes

$$T_{xu} := (sI - A)^{-1} B W_i(s) \tag{4.19}$$

$$T_{yx_0} := W_o(s) C (sI - A)^{-1} \tag{4.20}$$

and the frequency weighted Grammians becomes

$$\Sigma_c = \frac{1}{2\pi} \int_{-\infty}^{\infty} T_{xu}(i\omega) T_{xu}(i\omega)^* d\omega, \tag{4.21}$$

$$\Sigma_o = \frac{1}{2\pi} \int_{-\infty}^{\infty} T_{yx_0}(i\omega)^* T_{yx_0}(i\omega) d\omega, \tag{4.22}$$

Again, finding a balancing transformation such that the frequency weighted Grammians Σ_c, Σ_o are equal and diagonal, the transformation can be used to obtain the frequency weighted balanced state space realization and the truncated model can be obtained in the same way as for the unweighted case. The truncated system is only guaranteed to be stable if one sided frequency weights are used [15].

4.3 Implementation and Results

Because the discretized model has a pole at the origin it can not be used directly as a frequency weight because the frequency weighted Grammians will not converge with a frequency weight that is not strictly stable. Hence the system matrix of the discretized model is changed by moving all the poles into the left half plane before being used as a frequency weight:

$$A_\epsilon = A - I\epsilon \tag{4.23}$$

Frequency weighted model reduction on the Kalman filter is performed with the inputs of the Kalman filter (i.e. the measurement vector y) weighted by the modified plant and the disturbance frequency weight. That is, $W_i = \tilde{P}_\epsilon^N(s) W_d(s)$, and $W_o = 1$.

Kalman filters are designed for LTI realizations of the discretized model with from 2 to 100 control volumes. The resulting Kalman filters are of order $n = 2N + 5$, i.e. $F^N, N \in [2, 100]$. Then reduced order Kalman filters of order 1 through 205 are obtained through frequency weighted model reductions of F^{100},F^{50} and F^{25} corresponding to $\tilde{P}^{100}$, $\tilde{P}^{50}$ and $\tilde{P}^{25}$ respectively. The performance is computed as explained in section 4.1.4.

The results are shown in Fig. 4.3. The performance of F^{100} on $\tilde{P}^{100}$, refereed to as the nominal performance can be viewed as a bound on possible performance increase by increasing the number of control volumes. It can be seen that to achieve good performance it is important to start with a sufficiently high order discretization. Then the filter can be reduced to a low order without compromising performance. We note that when the Kalman filters are reduced sufficiently the performance is not increased by starting out with a higher order discretization. I.e. if one are satisfied with a standard deviation in the estimation error of $0.3[bar]$ starting out with a 50 control volume discretization is sufficient. Simulation results are included in the appendix A.2.

In the implementation of the frequency weighted model reduction the WOR-toolbox for MATLAB [26] was used.

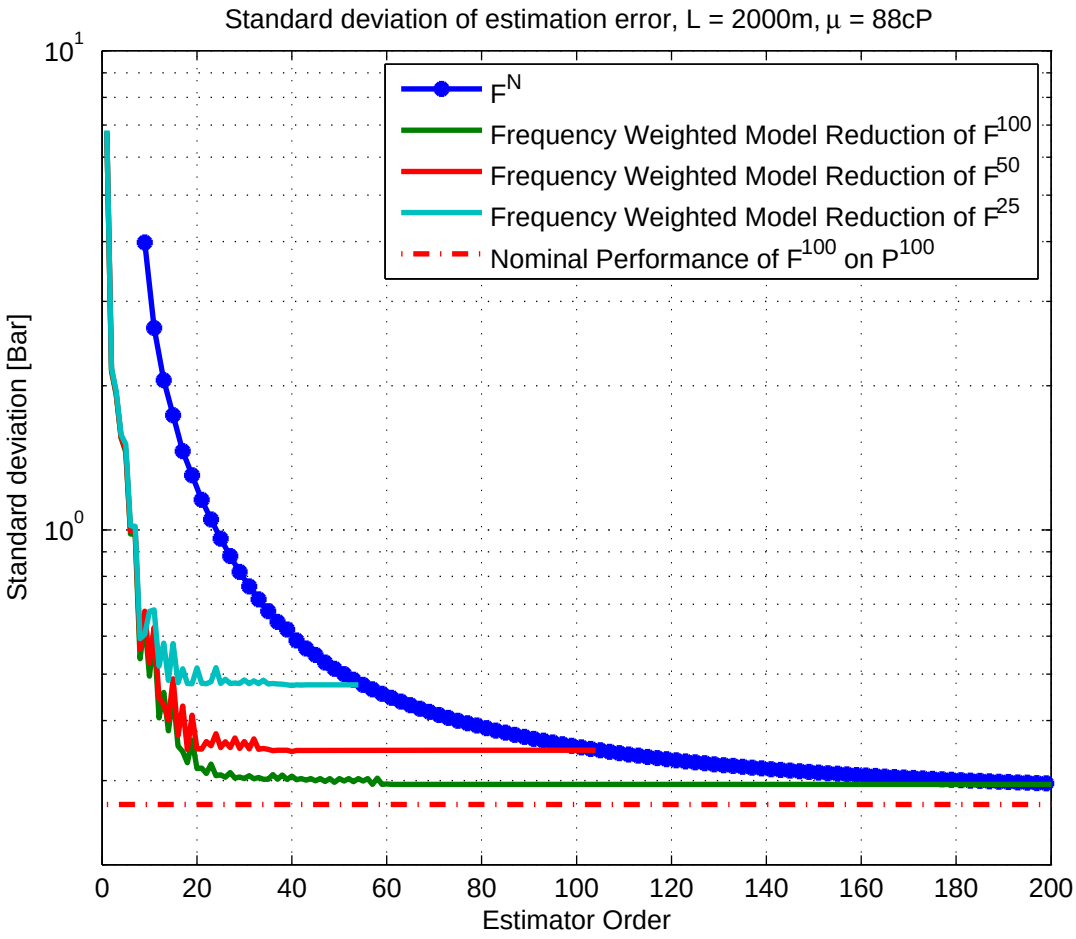

Figure 4.3: Comparison of filter performance of the two different approaches of obtaining a low order Kalman Filter. Performance is calculated based on irrational transfer function. Nominal performance is performance of the full order Kalman filter on the full order nominal plant and can be seen as a lower bound on performance.

Chapter 5

Conclusions and Further Work

In this thesis it was shown that the earlier work done on the attenuation of the periodic heave disturbance have been done based on an incomplete model, in that it did not include the effect of mud clinging to the drill string. By presenting a new model that includes this effect and deriving the frequency response of this model in the case of Newtonian drill mud, it was shown that the mud clinging effect becomes significant for drill muds with high viscosity, but that the old model will work for low viscosity drill muds.

The effect of non-Newtonian drill muds was also discussed. Analytical solutions for this case exists but they are given by implicit relations which are difficult to use in controller and estimator design. In what cases the viscous friction of non-Newtonian drill muds can be approximated with a linear relation should be investigated further.

For the case of Newtonian drill muds, the well model can effectively be approximated by a finite dimensional LTI system through spatial discretization. It was shown that to get good performance of an estimator designed based on such an approximation, it is important to start out with a high order discretization. The same is true for controller design. It was also shown that the estimator can be reduced to order 20 without significant loss in performance through the use of frequency weighted model reduction techniques.

The reduced order estimator of order 20 had a standard deviation in the estimation error of 0.32 [Bar] for typical magnitudes of measurement noise and heave disturbance in a MPD configuration. Employing this estimator in feedback loop with a controller will yield a theoretical bound on performance of the regulation error standard deviation of 0.32 [Bar]. In practice model uncertainty must also be taken into account which is something that has not yet been investigated.

Performance can be improved by increased knowledge of the frequency of the heave disturbance. The estimator designed in this thesis considered the full frequency spectrum calculated by three hours of floater heave data and therefore uses a broad frequency weight on the disturbance. To what degree the frequency weight of the heave disturbance can be narrowed, which would yield increased performance, should be investigated further.

Bibliography

[1] F. E. Crespo. Experimental study and modeling of surge and swab pressure for yield-power-law fluids. diploma thesis, University of Oklahoma, 2011.

[2] V. L. Streeter E. B. Wylie. *Fluid transients*. McGraw-Hill International Book Co., 1978.

[3] Olav Egeland and Jan Tommy Gravdahl. *Modeling and Simulation for Automatic Control*. Marine Cybernetics, 2002.

[4] J. E. Fontenot and R. K. Clark. An improved method for calculating swab and surge pressures and calculating pressures in a drilling well. *SPEJ*, pages 451–462, Feb. 1974.

[5] L. Imsland O.M. Aamo G. Kaasa, O.N. Stamnes. Intelligent estimation of dowhole pressure using a simple hydraulic model. In *IADS/SPE Managed Pressure Drilling and Underbalance Operations Conf. and Exhibition*, April. 2011.

[6] Kristian Gjerstad, Rune W. Time, and Knut S. Bjørkevoll. Simplified explicit flow equations for bingham plastics in couette poiseuille flow for dynamic surge and swab modeling. *Journal of Non-Newtonian Fluid Mechanics*, (0):55 – 63, 2012.

[7] Alexey; Kaasa Glenn-Ole; Rolland Nils Lennart Godhavn, John-Morten; Pavlov. Drilling Seeking Automatic Control Solutions. In *18th IFAC World Congress*, 2011.

[8] Alexey Pavlov Hessam Mahdianfar, Ole Morten Aamo. Attenuation of Heave-Induced Pressure Oscillations in Offshore Drilling Systems. In *American Control Conference (ACC)*, 2012.

[9] Alexey Pavlov Hessam Mahdianfar, Ole Morten Aamo. Suppressing heave-induced pressure fluctuations in MPD. In *IFAC Workshop - Automatic Control in Offshore Oil and Gas Production*, May 2012.

[10] Ulf Jakob F. Aarsnes Alexey Pavlov Ole Morten Aamo Ingar Skyberg Landet, Hessam Mahdianfar. Modeling for MPD Operations with Experimental Validation. In *IADC/SPE Drilling Conference and Exhibition, 6-8 March 2012, San Diego, California, USA*, 2012.

[11] A. Ellman J. Makinen, R. Piche. Fluid transmission line modeling using a variational method. *J. Dynamic Systems, Measuremnet, and Control*, pages 153 – 162, 2000.

[12] Humble Oil & Refining Co. J.A. Burkhardt. Wellbore pressure surges produced by pipe movement. *Journal of Petroleum Technology*, 13:595–605, 1961.

[13] A. Settari K. Aziz. *Petroleum reservoir simulation*. Applied Science Publishers (London), 1979.

[14] Glenn-Ole Kaasa. A simple dynamic model of drilling for control. 2000.

[15] John C. Doyle Kemin Zhou and Keith Glover. *Robust and Optiaml Control*. Prentice Hall, 1995.

[16] Ingar Skyberg Landet. Advanced modeling for managed pressure drilling. Project report, NTNU, December 2010.

[17] Ingar Skyberg Landet. Modeling and control for managed pressure drilling from floaters. diploma thesis, NTNU, June 2011.

[18] Hsu F. H. Lubinski, A. and K. G. Nolte. Surpressions transitoires dues au mouvement des colonnes de tubes dans les puits. *Oil & Gas Science and Technology - Rev. IFP*, 32(3):307–348, 1977.

[19] Goro Obinata and Brian D.O. Anderson. *Model Reduction for Control System Design*. Springer, 2001.

[20] J.-M. Godhavn E.H. Vefring O.Breyholtz, G. Nygaard. Evaluating control designs for co-ordinating pump rates and choke valve during managed pressure drilling operations. *Control Applications, (CCA) & Intelligent Control*, pages 731 – 738, 2009.

[21] Glenn-Ole; Imsland Lars Pavlov, Alexey; Kaasa. Experimental Disturbance Rejection on a Full-Scale Drilling Rig. In *8th IFAC Symposium on Nonlinear Control Systems (2010)*, 2010.

[22] Maarten Steinbuch Pepijn M. R. Wortelboer and Okko H. Bosgra. Iterative model and controller reduction using closed-loop balancing, with application to a compact disc mechanism. *Int. J. Robust Nonlinear Control*, 9:123–149, 1999.

[23] Enertech Engineering & Research R.F. Mitchell. Dynamic surge/swab pressure predictions. *SPE Drilling Engineering*, 3:325–333, 1988.

[24] A.S. Halal R.R. Wagner and Enertech Engineering & Research Co. M.A. Goodman. Surge field tests highlight dynamic fluid response. In *IADC/SPE Drilling Conference*, Feb. 1993.

[25] Y. Wang and G. A. Chukwu. Application of unsteady couette flow of non-newtonian power-law fluids in concentric annular wellbore. *Journal of Petroleum Science and Engineering*, 17:229–235, 1997.

[26] P. M. R Wortelboer. *WOR-toolbox:toolbox for Weighted Order Reduction*, 1998 (downloaded October, 2011).

Appendix A

Additional Figures

A.1 Frequency Response Functions

The frequency response of P_{12} (i.e. from v_d to p_c) is plotted in Fig. A.1 and Fig. A.2 with the physical properties shown in Table 3.1

A.2 Simulation Results

In this simulation the length of the well was 2000 meters and viscosity was $\mu = 88cP$. The simulation was performed with white measurement noise with standard deviations:

- Heave measurement noise standard deviation: 0.1 $[m/s]$
- Choke flow measurement noise standard deviation: 50 liters/min $[m^3/s]$
- Topside pressure measurement noise standard deviation: 0.1 $[Bar]$

It can be seen that there is a significant loss in performance between the 20th order estimator shown in Fig. A.3 and 6th order estimator shown in Fig. A.4. The estimation error corresponds well with the standard deviation of the error predicted by Fig. 4.3.

A.3 Unweighted Reduction and Reduce First Approach

In Fig. A.5 it can be seen how the reduce first model reduction approach yields bad results for the considered system and application. It can also be seen that the design first approach fails when appropriate weights are not used.

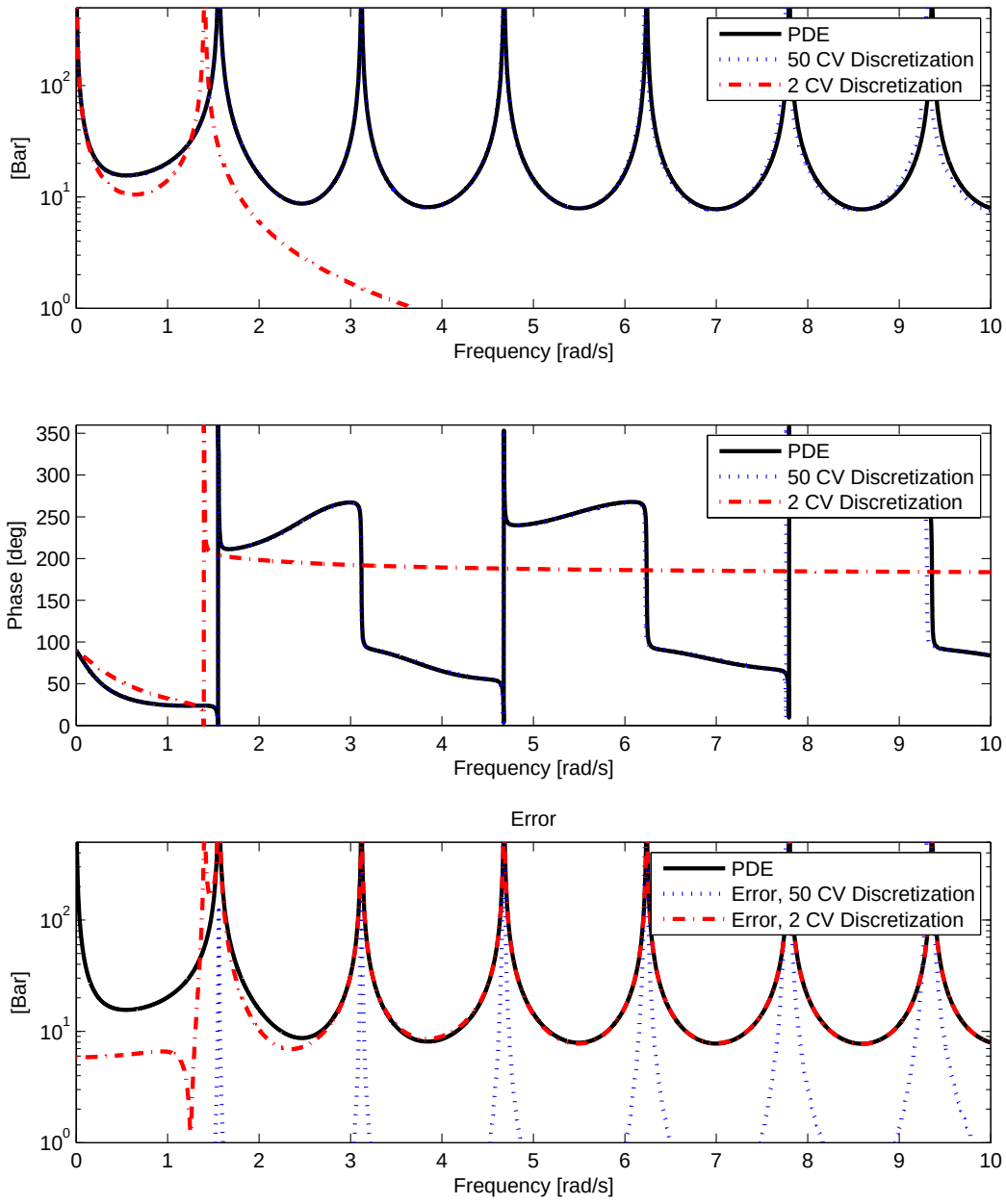

Figure A.1: Gain and phase of the irrational transfer function P_{21} evaluated on the imaginary axis compared with transfer function of the discretized version of the same PDE with 2 and 50 Control Volumes Respectively. The length of well is 2000 meters.

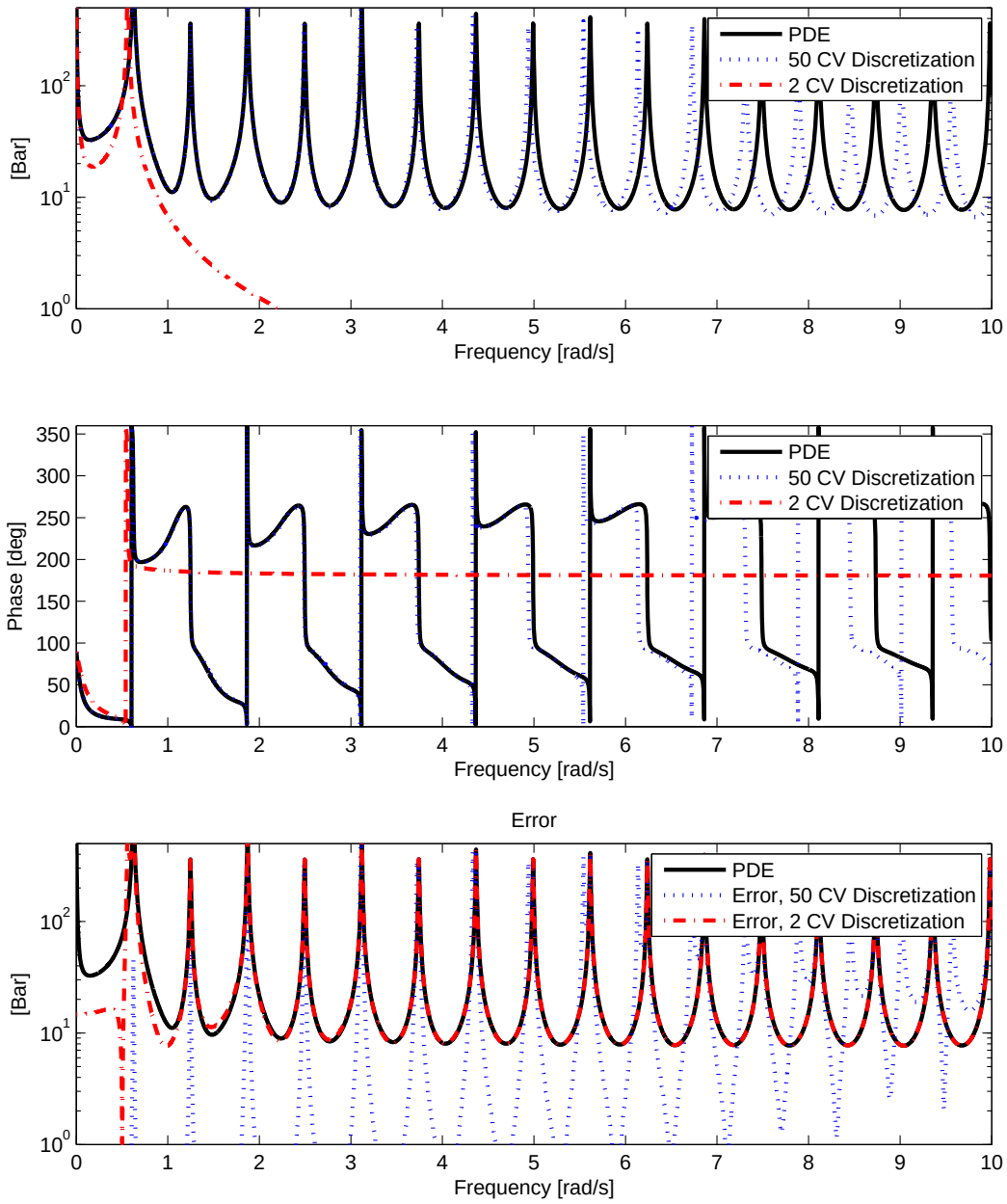

Figure A.2: Gain and phase of the irrational transfer function P_{22} evaluated on the imaginary axis compared with transfer function of the discretized version of the same PDE with 2 and 50 Control Volumes Respectively. The length of the well is 5000 meters.

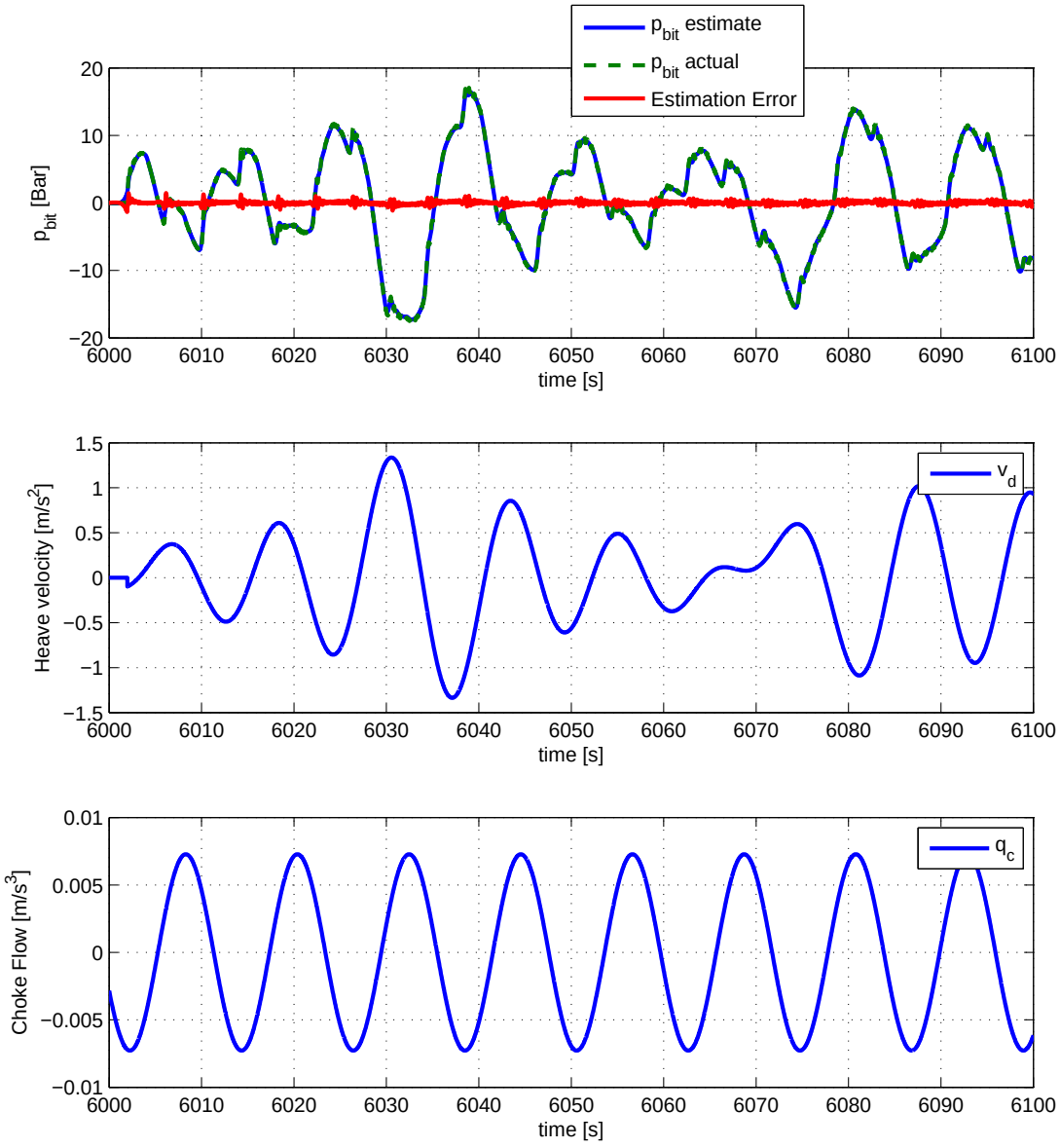

Figure A.3: Frequency reduced Kalman filter of order 20 simulated on a discretized model with 100 Control Volumes.

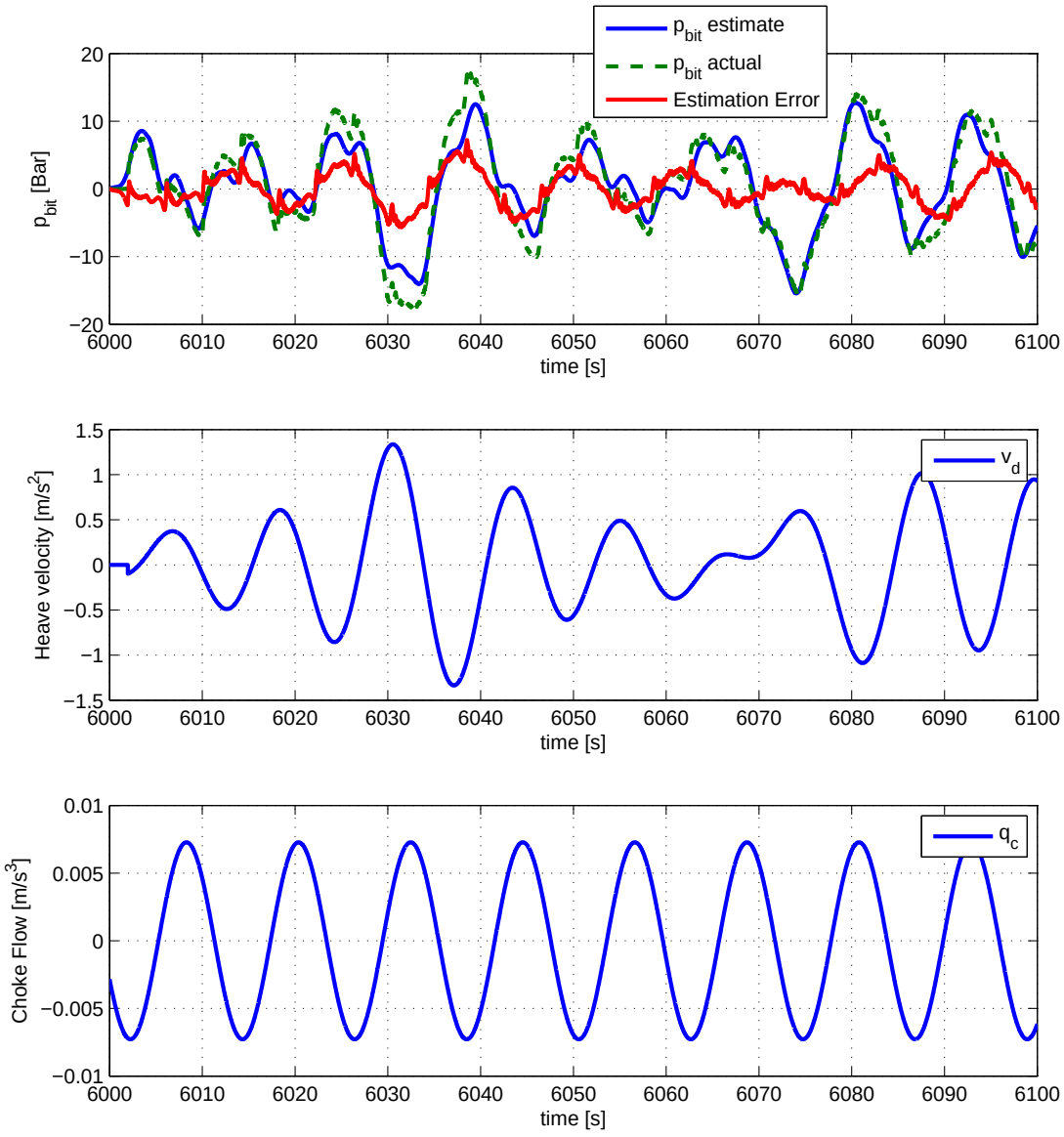

Figure A.4: Frequency reduced Kalman filter of order 6 simulated on a discretized model with 100 Control Volumes.

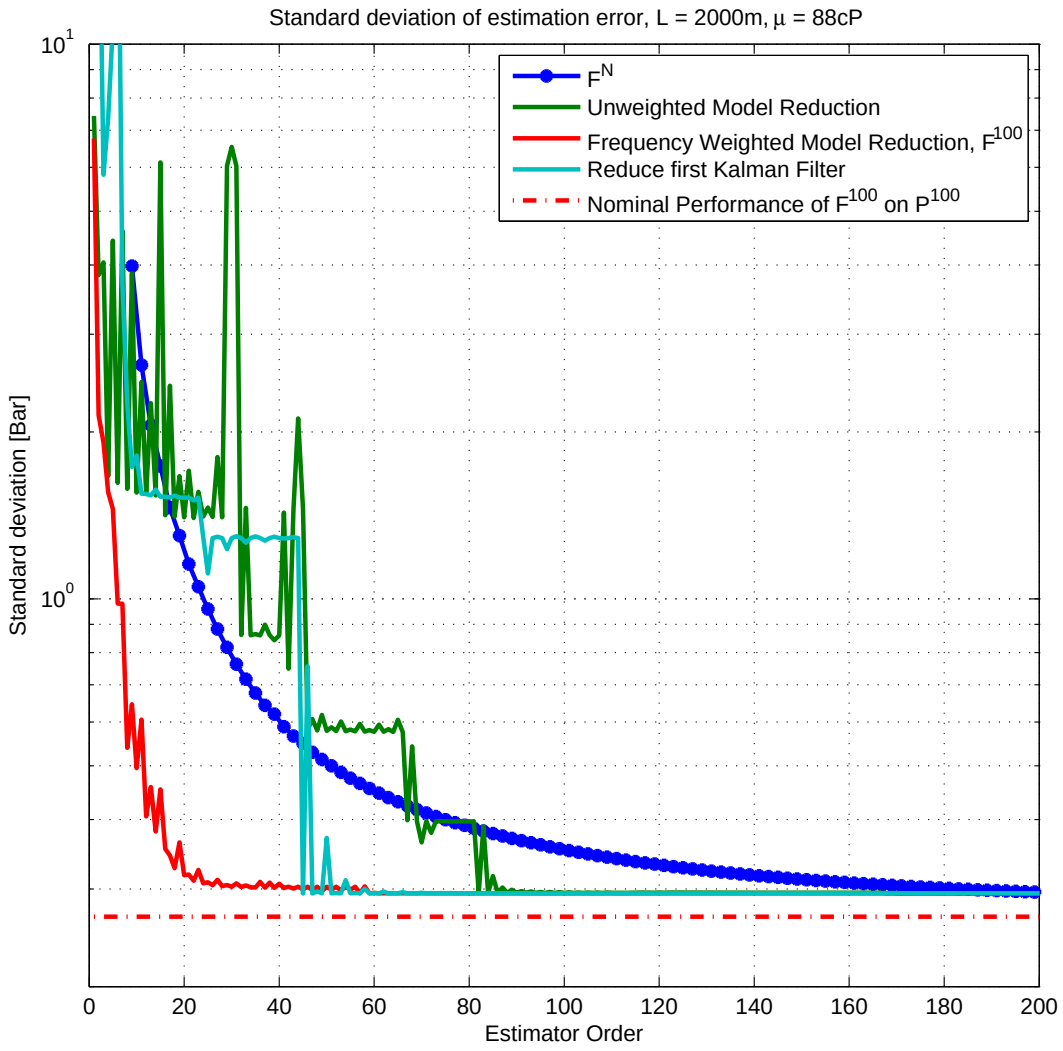

Figure A.5: Kalman Filter performance comparison including reduced first and unweighted model reduction.

Appendix B

Conference Paper

The Following Paper was submitted to 2012 Australian Control Conference.

Quantifying Error Introduced by Finite Order Discretization of a Hydraulic Well Model*

Ulf Jakob F. Aarsnes[1], Ole Morten Aamo[1] and Alexey Pavlov[2]

***Abstract*— A model of a hydraulic transmission line used to model the pressure fluctuations in a drilling well caused by vertical movement of the drill string (heave) is presented. Using the Laplace transform and appropriate boundary conditions the transfer function of the model is derived. The model uses the heave disturbance and controlled flow into the drilling well as inputs, and the measured topside pressure and controlled downhole pressure as output. A rational approximation of the system using spatial discretization is obtained using the Control Volume method. The error introduced by the discretization is analysed in the frequency domain. Then, the discretized models with varying number of control volumes are used for Kalman filter and LQG design. The performance of the Kalman filter and LQG when the well is subjected to the heave disturbance is compared over different number of control volumes and well lengths. Finally, it is shown how the robust performance of the LQGs can be checked w.r.t. the plant uncertainty introduced by the discretization.**

I. Introduction to MPD and the Heave Attenuation Problem

In drilling operations performed in the oil and gas industry a fluid called mud is pumped down through the drill string and flows through the drill bit in the bottom of the well, see Fig. 1. If the pressure in the mud at the bottom of the well is too low the well can collapse trapping the drill string, and if the pressure exceeds a certain threshold it can fracture the well. Hence, it is important to control the mud pressure in the well. In Managed Pressure Drilling (MPD) operations this is achieved by sealing the well and releasing mud from the well through a control choke. A back pressure pump allows the pressure to be controlled even when the main pump is stopped. Thus, the pressure in the bottom of the well can be regulated to a desired set-point. This approach has proven successful when drilling from stationary platforms and results on MPD control can be found in papers such as [8],[1]. MPD from floating drilling rigs, however, still face significant challenges due to the wave induced vertical motion of the floating drilling rig (known as heave). During normal drilling the heave motion of the drilling rig is decoupled from the drill string by compensation techniques. However, when the drill string is to be extended by a drill string connection it is rigidly connected to the floater. It will then act as a piston in the well creating pressure oscillations

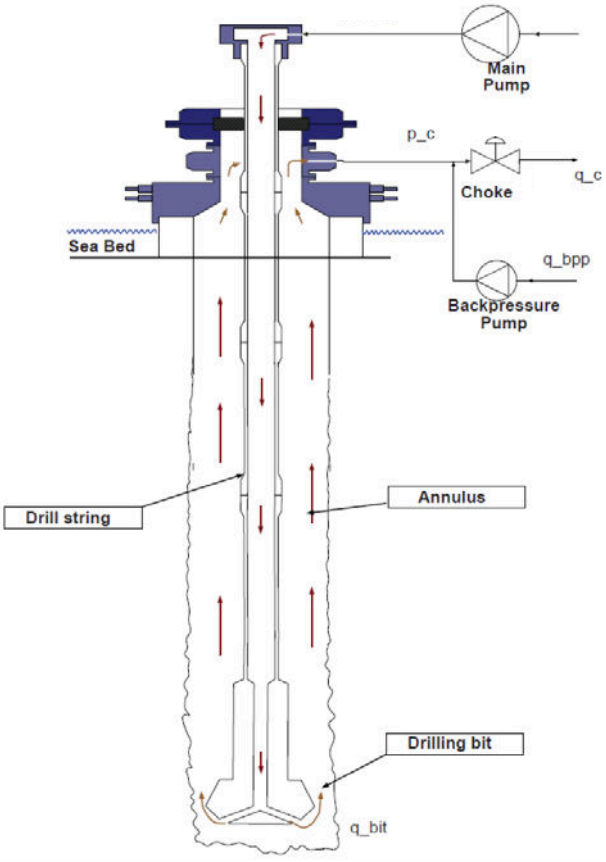

Fig. 1. Well configuration for MPD. Shown by courtesy of Statoil ASA

which may exceed the upper or lower pressure thresholds one wishes to enforce. It is therefore desirable to utilize active control of the topside choke to compensate for the pressure changes due to the heave motion. In this scenario, the main pump is disconnected and there is no flow between the annulus and the drill string (the drill bit is equipped with a one-way valve which prevents back flow from the annulus into the drill string.) Hence the dynamics of interest is the pressure dynamics in the annulus. In [3] a simple hydraulic model, developed in [7] using a single control volume, was used for controller design. However, in full scale testing it was shown that the controller was unable to successfully compensate for the heave disturbance. In [2] it was suggested (and shown in simulations) that a higher order discretization of the model can be used to improve accuracy. But, since the order of the controllers and observers depend on the order of

*This work was supported by Statoil ASA

[1]U. J. F. Aarsnes and O. M. Aamo are with the Department of Engineering Cybernetics, Faculty of Information Technology, Mathematics and Electrical Engineering, Norwegian University of Science and Technology (NTNU), Trondheim, Norway ulfjakob at stud.ntnu.no, aamo at ntnu.no

[2]A. Pavlov is with the Department of Intelligent Well Contruction, Statoil Research Centre, Porsgrunn, Norway.

Preprint submitted to 2012 Australian Control Conference. Received May 7, 2012.

the model, it is desirable to have the model of as low order as possible. Therefore we would like to be able to determine what order of the model is required to achieve the required accuracy.

In this paper we will show how accuracy is improved by increasing the number of control volumes. The result allows one to quantify the accuracy of the discretized model as a function of the discretization order, for a given set of physical well properties. The result can be used in open loop, with an estimator and in closed loop with a controller. Since the error introduced by the discretization is quantified, we can also check the robust stability properties for a given controller. Thus one can use this result to determine the lowest order of the model which results in a controller with sufficient accuracy and robustness.

The paper is organized in the following way: the hydraulic well model is presented in Section II. The discretized model is presented in Section III. Finally, in Section IV it is shown how the error resulting from the discretization can be calculated when the discretized model is used for controller or estimator design.

II. The Hydraulic Well Model

Considering a single phase flow in the annulus, the pressure dynamics can be modelled as a hydraulic transmission line. Following the derivation in [4], the dynamic model is developed from the mass and momentum balance of a differential control volume Adx. x is distance along the well with $x = 0$ being at the bottom, and t is time. Linearising around $q = 0$ and $\rho = \rho_0$ the model becomes

$$\frac{\partial p(x,t)}{\partial t} = -\frac{\beta}{A}\frac{\partial q(x,t)}{\partial x} \tag{1}$$

$$\frac{\partial q(x,t)}{\partial t} = -\frac{A}{\rho_0}\frac{\partial p(x,t)}{\partial x} - \frac{F}{\rho_0} + Ag\cos\big(\alpha(x)\big) \tag{2}$$

where $p(x,t), q(x,t)$ are mean pressure and flow rate and A, β, α are the cross section area of the well, bulk modulus of the drilling mud and well inclination respectively. In the following we will omit the (x,t) where the dependency is obvious. Continuing the assumption that the flow is small (i.e. q is close to zero) and referring to tests done in [2], we assume linear friction: $F = kq$. As (1)-(2) is linear the constant term due to the gravitational force will not effect the dynamics of the system, only the steady state. By taking p to be defined as deviations from the steady state pressure at $t = 0$, we can discard the term due to gravity. This distributed parameter system is based on the following assumptions [5].

- The fluid obeys Stokes' law, i.e. the fluid is Newtonian.
- The flow is laminar, i.e., the Reynolds number is 2300 or less.
- The flow is axisymetrical. This assumption implies that the conduit is straight, although the equations works when the well have a relatively small radius of curvature.
- Motions in the radial direction is negligible. This implies that the longitudinal velocity component is much greater than the radial component and that pressure is constant across the cross section.
- Nonlinear convective acceleration terms are negligible. This assumption is valid when the mud velocity is much smaller than the speed of sound in the mud.
- Material properties are constant.
- The pipe walls are rigid. This assumption is likely to be incorrect so β should be increased to some effective bulk modulus of the mud in the annulus to reflect the elasticity of the walls.
- Thermodynamic effects are negligible.
- Friction is a linear function of flow.

A. Laplace Transformed System

Using subscript notation to denote partial derivatives , (1)-(2) can be written as

$$p_t + \frac{\beta}{A}q_x = 0 \tag{3}$$

$$q_t + \frac{A}{\rho_0}p_x + kq = 0 \tag{4}$$

Differentiating (3) w.r.t. to x and (4) w.r.t. t;

$$p_{tx} + \frac{\beta}{A}q_{xx} = 0 \tag{5}$$

$$q_{tt} + \frac{A}{\rho_0}p_{xt} + kq_t = 0 \tag{6}$$

Inserting (5) for p_{xt} in (6). This gives

$$q_{tt} - c^2 q_{xx} + kq_t = 0, \quad c = \sqrt{\frac{\beta}{\rho_0}} \tag{7}$$

This is the one dimensional wave equation with dissipation, and c is the speed of sound. By utilizing the Laplace transform we want to derive the transfer function of the system. Taking the Laplace transform of (7), denoting the Laplace transformed function by $\hat{q}$, and assuming steady-state at $t = 0$ (i.e. that $q(x,0) = 0$), we get

$$\hat{q}_{xx} - \hat{q}\frac{1}{c^2}(s^2 + sk) =: 0 \tag{8}$$

This is a second order Ordinary Differential Equation and can be solved for $\hat{q}(x,s)$. Defining $\gamma^2 := \frac{1}{c^2}(s^2 + sk)$, the solution is

$$\hat{q}(x,s) = \ C_1 \sinh(\gamma x) + \ C_2 \cosh(\gamma x) \tag{9}$$

where C_1, C_2, are integration constants that have to be solved from the boundary conditions.

B. Solving for Boundary Conditions

The boundary conditions are the flow into the bottom of the well, and flow out of the top of the well. Assuming that the movement of the drilling bit can be modelled as a volumetric flow into the bottom of the well, we have $\hat{q}(0,s) = A_d\hat{v}_d(s)$, where A_d is the cross section area of the drilling bit. Denoting the flow through the choke at the

top of the well by q_c, we have $\hat{q}(L,s) = \hat{q}_c(s)$. Enforcing these boundary conditions on (9), we get

$$C_2 = A_d \hat{v}_d(s) \tag{10}$$

$$C_1 = \frac{\hat{q_c}}{\sinh(\gamma L)} - \frac{A_d \hat{v}_d(s)}{\tanh(\gamma L)} \tag{11}$$

Substituting C_1 and C_2 into (9) we get

$$\hat{q}(x,s) = \hat{q}_c(s)\frac{\sinh(\gamma x)}{\sinh(\gamma L)} \tag{12}$$

$$+ A_d \hat{v}_d\Big(\cosh(\gamma x) - \frac{\sinh(\gamma x)}{\tanh(\gamma L)}\Big) \tag{13}$$

Differentiating with respect to x, we get

$$\hat{q}_x(x,s) = \hat{q}_c(s)\gamma\frac{\cosh(\gamma x)}{\sinh(\gamma L)} \tag{14}$$

$$+ A_d \hat{v}_d(s)\gamma\Big(\sinh(\gamma x) - \frac{\cosh(\gamma x)}{\tanh(\gamma L)}\Big) \tag{15}$$

and inserting into the Laplace transform of (3), we obtain

$$\hat{p}(x,s) = -\frac{\beta}{sA}\hat{q}_x(x,s) \tag{16}$$

where $p(x,0) = 0$ assuming the well dynamics are at steady state at $t = 0$ (i.e. $p(x,t) = 0$). Now, defining

$$P_1(s) := \frac{\beta\gamma}{As\tanh(\gamma L)} \tag{17}$$

$$P_2(s) := \frac{\beta\gamma}{As\sinh(\gamma L)} \tag{18}$$

we can write the well model as a system with inputs v_d, q_c and outputs p_{bit}, p_c.

$$\begin{bmatrix} p_{bit} \\ p_c \end{bmatrix} = \begin{bmatrix} P_1 A_d & P_2 \\ P_2 A_d & P_1 \end{bmatrix} \begin{bmatrix} v_d \\ q_c \end{bmatrix} \tag{19}$$

III. Discretized Model

In the above section the hydraulic transmission line was described as a distributed parameter model, and its corresponding irrational transfer function was derived. For simulation and design purposes it is often necessary to have the system modelled by a set of ordinary differential equations (ODEs). One way of doing this is by truncating the series expansions of the irrational transfer function (19) which is discussed in [5]. Here we will instead consider the discretized model derived by considering a series of control volumes. This approach is popular since it is intuitive and it is easy to model wells where the physical properties, such as cross section area and bulk modulus, changes over the length of the well. Such a model based on the Helmholtz resonator model will be used here, following the derivation from [4].

A. Impedance Model

Using the same boundary conditions as in (10)–(11) the input variables at the top and the bottom of the well is q_c and v_d respectively. Define volume 1 to be at the bottom of the well, volume N to be at the top of the well and volume i centered at $x_{j-1/2} = (j-1/2)l$. The volumes have length l, and the well has length $L = Nl$. The dynamic order of the resulting systems is $2N-1$. The model is

$$\dot{p}_j = \frac{\beta}{Al}(q_{j-1} - q_j), \quad j = 1, \ldots, N$$

$$\dot{q}_j = \frac{A}{l\rho_0}(p_j - p_{j+1}) - kq_j, \quad j = 1, \ldots, N-1$$

$$q_0 = A_d v_d, \quad q_N = q_c$$

In this model p_j for $j = 1, \ldots, N$ is defined as deviation from the steady state pressure distribution at $t = 0$. Note that when N tends to infinity, l will tend to zero and the model will converge to the PDE (1)–(2).

TABLE I

The physical properties of the well

Parameter	Value
Length of well	$2000, 5000, 10000[m]$
Cross section area of well	$0.0273[m^2]$
Cross section area of drilling bit	$0.0148[m^2]$
Bulk Modulus	$1.4 * 10^9[Pa]$
Drilling Mud Mass Density	$1420[kg/m^3]$
Linear Friction Coefficient	$0.4684[kg/(m^3 s)]$

B. Comparison to the PDEs Frequency Response

In the following, a typical drilling well is considered with the physical properties shown in Table I. To save space, only the frequency response of P_1 is plotted in In Fig. 2 and Fig. 3, but the analysis is qualitatively the same for P_2. In Fig. 2 and Fig. 3 it can be seen how the discretization based on 2 control volumes quickly deteriorates in accuracy as frequency increases. The 50 control volumes discretization shows that high accuracy can be achieved at the cost of increased model complexity. We also note that when the length of the well increases, accuracy deteriorates as the length of each control volume increases.

C. Resonance Frequencies

The irrational transfer functions (17) and (18) have damped resonance peaks at their Resonance frequencies which occurs when $\sinh(\gamma l)$ is zero. Using the approximation

$$\frac{L}{c}\sqrt{-\omega^2 + k\omega i} \approx \frac{L}{c}\big(\omega i + \frac{k}{2}\big) \tag{20}$$

which is valid when ω is not close to 0, we can write

$$\sinh\big(\frac{L}{c}\big(\omega i + \frac{k}{2}\big)\big) = \tag{21}$$

$$\sinh\big(\frac{Lk}{2c}\big)\cos\big(\frac{L\omega}{c}\big) + i\cosh\big(\frac{Lk}{2c}\big)\sin\big(\frac{L\omega}{c}\big) \tag{22}$$

It can be seen that the damped resonance frequencies occurs at $\omega_{r,j} = \frac{j\pi c}{l}$, $j = 1, 2, \ldots$, and that as $\frac{Lk}{c}$ becomes larger the resonance decreases in magnitude.

For comparison, the resonance frequencies of the discretized system can be found by calculating the eigenvalues of the system matrix. The system matrix has an eigenvalue in 0 and $N-1$ pairs of complex conjugated eigenvalues with real part $-\frac{k}{2}$ and complex part equal the resonance frequency in rad/s of the corresponding damped resonance peak. The

TABLE II

RESONANCE FREQUENCIES EVALUATED FOR THE PROPERTIES GIVEN IN TABLE I WITH $L = 2000m$

	$\omega_{r,1}$	$\omega_{r,2}$	$\omega_{r,3}$	$\omega_{r,4}$
P	$\frac{\pi}{L}\sqrt{\frac{\beta}{\rho_0}} = 1.56$	$2\frac{\pi}{L}\sqrt{\frac{\beta}{\rho_0}} = 3.12$	$3\frac{\pi}{L}\sqrt{\frac{\beta}{\rho_0}} = 4.68$	$4\frac{\pi}{L}\sqrt{\frac{\beta}{\rho_0}} = 6.24$
$\tilde{P}^2$	$2\frac{\sqrt{\frac{8\beta}{\rho_0}-\frac{k^2L^2}{2^2}}}{2L} = 1.38$			
$\tilde{P}^3$	$3\frac{\sqrt{\frac{4\beta}{\rho_0}-\frac{k^2L^2}{3^2}}}{2L} = 1.47$	$3\frac{\sqrt{\frac{12\beta}{\rho_0}-\frac{k^2L^2}{3^2}}}{2L} = 2.57$		
$\tilde{P}^4$	$4\frac{\sqrt{\frac{4(2-\sqrt{2})\beta}{\rho_0}-\frac{k^2L^2}{4^2}}}{2L} = 1.50$	$4\frac{\sqrt{\frac{8\beta}{\rho_0}-\frac{k^2L^2}{4^2}}}{2L} = 2.80$	$4\frac{\sqrt{\frac{4(2+\sqrt{2})\beta}{\rho_0}-\frac{k^2L^2}{4^2}}}{2L} = 3.66$	
$\tilde{P}^5$	$5\frac{\sqrt{\frac{2(3-\sqrt{5})\beta}{\rho_0}-\frac{k^2L^2}{5^2}}}{2L} = 1.52$	$5\frac{\sqrt{\frac{2(5-\sqrt{5})\beta}{\rho_0}-\frac{k^2L^2}{5^2}}}{2L} = 2.91$	$5\frac{\sqrt{\frac{2(3+\sqrt{5})\beta}{\rho_0}-\frac{k^2L^2}{5^2}}}{2L} = 4.01$	$5\frac{\sqrt{\frac{2(5+\sqrt{5})\beta}{\rho_0}-\frac{k^2L^2}{5^2}}}{2L} = 4.72$

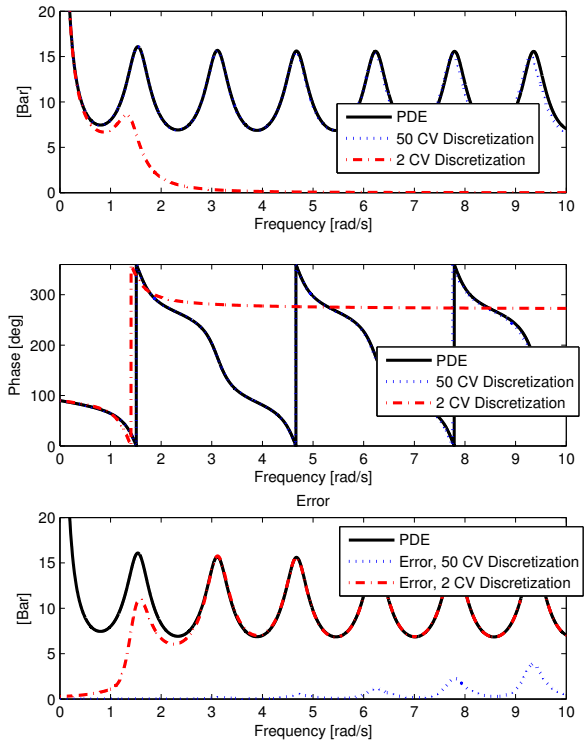

Fig. 2. Gain and phase of the irrational transfer function P evaluated on the imaginary axis compared with transfer function of the discretized version of the same PDE with 2 and 50 Control Volumes Respectively. The length of well is 2000 meters.

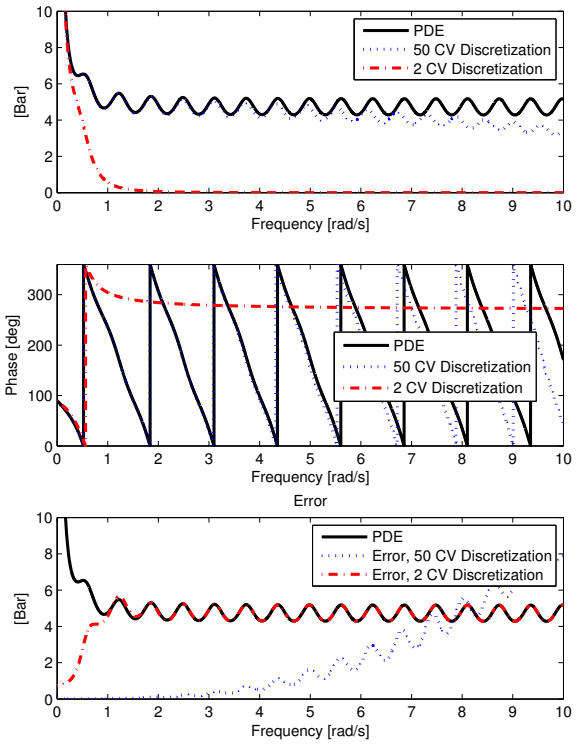

Fig. 3. Gain and phase of the irrational transfer function P evaluated on the imaginary axis compared with transfer function of the discretized version of the same PDE with 2 and 50 Control Volumes Respectively. The length of the well is 5000 meters.

resonance frequencies of the discretized systems of 2 to 5 control volumes can be found in Table II.

IV. EXAMPLES ON ESTIMATOR AND CONTROLLER DESIGN

Now we will show two examples of how to quantify the error introduced by the discretization in closed loop.

A. The Heave Disturbance

As was seen in Fig. 2 and 3, the accuracy of the discretized model is dependent on the required bandwith of the system. The velocity of the heave motion of a floating rig will in a given situation have its energy centered around a main frequency component in the frequency spectrum. The frequency spectrum of the heave motion of a floating rig based on 3 hours of logged data can be seen in Fig 4. The main frequency component is located at $0.5[rad/s]$.

B. Quantifying Error in Estimator Design

In this application we are considering a disturbance with known frequency. The estimator is designed as a Kalman filter with an internal model of the heave disturbance so as

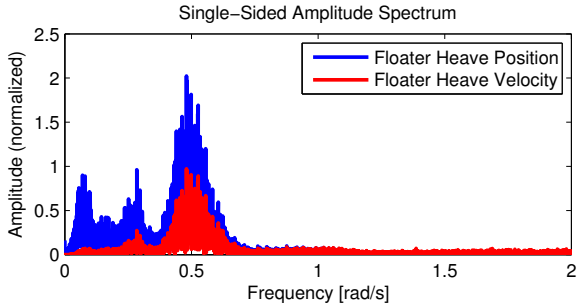

Fig. 4. Blue line is the empirical amplitude spectrum of the heave of a floater measured over three hours. The red line is the amplitude spectrum of the floater speed.

to be able to estimate the downhole pressure based on the measurement of the topside pressure. In the Kalman filter design, the relative disturbance to noise weighting is based on the following typical values for the heave disturbance and pressure measurement noise standard deviation

$$\begin{array}{rr} \text{Max heave velocity:} & 1[m/s] \\ \text{Noise Standard Deviation:} & 0.1[Bar] \end{array}$$

The design and error calculations are carried out in the following way. A state space realization $\tilde{P}^N(s)$ is made of the discretized model with N Control Volumes. A Kalman filter $F_N(s)$ with an internal model of the disturbance at the assumed known frequency is designed for the discretized model. Recall that the irrational transfer functions were denoted by $P_1(s),\ P_2(s)$, i.e.

$$p_{bit} = P_1(s)A_d v_d \tag{23}$$
$$p_c = P_2(s)A_d v_d \tag{24}$$

We evaluate the performance of the estimator $\hat{p}_{bit} = F_i(s)p_c$ by looking at the transfer function of the estimation error

$$e = p_{bit} - \hat{p}_{bit} = (P_1(s) - F_N(s)P_2(s))A_d v_d \tag{25}$$

By calculating the complex values of $P_1(s = i\omega), P_2(s = i\omega)$, the frequency response of the estimation error can be calculated by using (25). Plots of the performance of the resulting filters can be seen in Fig. 5 and Fig. 6. It can be seen that the estimation error decreases as the number of control volumes in the discretized model is increased. We also note that for the considered disturbance frequency of $0.5[rad/s]$ the estimation error increases significantly as the length of the well is increased. Both of these conclusions is as expected for the discretization procedure used.

Some controller and estimator designs may be difficult for high order models. For long wells in particular, this may necessitate the use of model reduction procedures as suggested in [2], or alternatively, doing controller/estimator design directly on the distributed system (1)-(2). This last approach is investigated in [9] and [10].

C. Quantifying Error in Controller Design

In this section we will show how the error dynamics of the irrational transfer function can be computed in closed loop

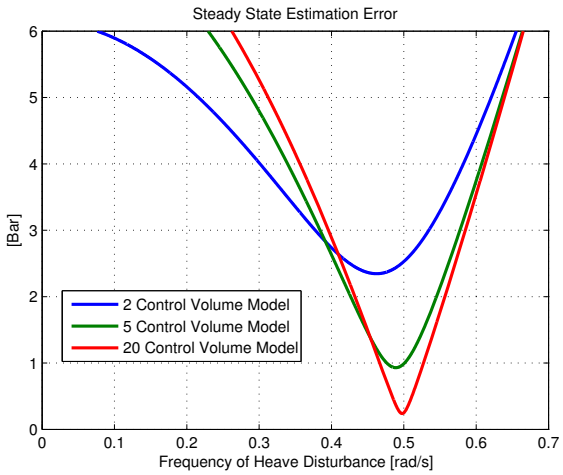

Fig. 5. Frequency response plot of the estimation error of downhole pressure for a sinusoidal heave disturbance with peak velocity of 1 meters per second. The estimators have been design to yield perfect estimation at 0.5 [rad/s] for the discretized model. The length of the well is 2000 meters.

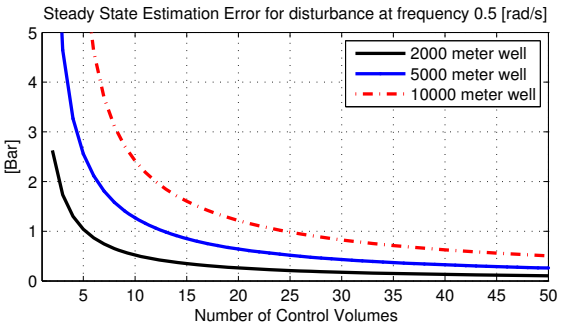

Fig. 6. Estimation error of the downhole pressure for a sinusoidal heave disturbance with peak velocity of 1 meters per second and frequency of 0.5 rad per second. The estimators have been designed to yield perfect estimation for this frequency for the corresponding discretized model.

with a controller. For this purpose we may design an LQG controller K_N for the Nth control volume discretization of the system; $\tilde{P}^N$. For the Kalman filter part of the LQG we use the same values for measurement noise and disturbance variance as in section IV-B. For the LQR state feedback, we want a state feedback which minimizes the cost function $J = \int_0^\infty p_{bit}^2 + \rho q_c^2 dt$. Through trial and error a weighting of $\rho = 1e4$ was found to result in expected performance and a stable controller.

To analyze the performance of the LQG in more realistic conditions, the following frequency weight is used for the heave disturbance.

$$W_d(s) = \frac{0.12(s - 0.01)}{(s^2 - 0.02s + 0.0251)(s - 1)} \tag{26}$$

The frequency response of W_d is shown in Fig. 7. The resulting configuration is shown in Fig. 8.

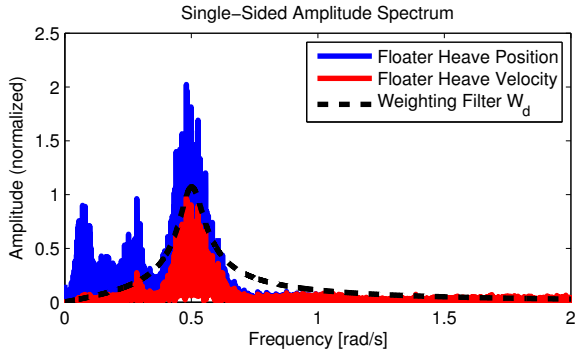

Fig. 7. Blue line is the empirical amplitude spectrum of the heave of a floater. The red line is the amplitude spectrum of the floater speed. The black line is the amplitude of the frequency response of the weighting filter W_d.

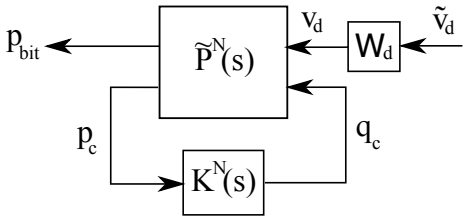

Fig. 8. Weighted feedback interconnection for LQG design.

The closed loop system can be written as

$$P(s) =: \begin{bmatrix} P_1 A_d & P_2 \\ P_2 A_d & P_1 \end{bmatrix} \tag{27}$$

$$\begin{bmatrix} p_{bit} \\ p_c \end{bmatrix} = P(s) \begin{bmatrix} v_d \\ q_c \end{bmatrix} \tag{28}$$

$$q_c = K_N(s) p_c \tag{29}$$

With this interconnection it can be shown that the transfer function of the downhole pressure from the heave disturbance is

$$p_{bit} = \left(P_1 + K_N \frac{P_2^2}{1 - P_1 K_N}\right) A_d v_d =: T_{zw}^N v_d \tag{30}$$

The performance of this controller designed for $N = 2, 5, 20$ can be seen in Fig 9. It is clear that when too few control volumes are used in the discretization, the controller is unable to attenuate the disturbance at the correct frequency. The weighted $\mathcal{H}_2$ norm of the closed loop system can also be computed. It can be interpreted as the standard deviation of the downhole pressure when the disturbance has the amplitude spectrum of W_d. We have

$$\text{Standard deviation } p_{bit} = ||T_{zw}^N W_d||_2 \tag{31}$$

Values of the computed standard deviation of p_{bit} for different number of control volumes and well lengths are shown in Fig. 10. In managed pressure drilling operations we wish to keep the downhole pressure within $\pm 2.5[Bar]$ of the setpoint. We can see that this is achieved for $N \geq 3$ for a well of 2000 meters. When the length of the well is increased to 5000 meters a significant increase in N is required to maintain acceptable performance. For the 10000 meters long

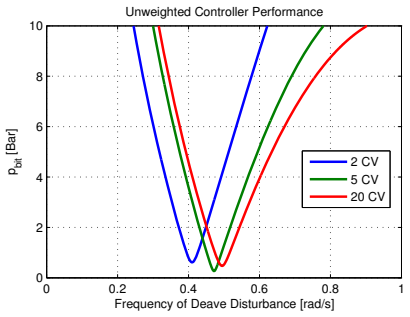

Fig. 9. Unweighted Frequency response plot of p_{bit} with v_d as input for LQGs designed with discretized models with different number of CVs. v_d has a peak amplitude of 1 meters per second. Lenght of the well is 2000 meters.

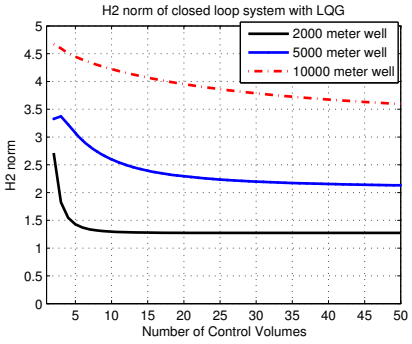

Fig. 10. Weighted $\mathcal{H}_2$ norm of the closed loop system. The system is closed with LQG controllers designed with different number of Control Volumes.

well, acceptable performance is not achieved for $N \leq 50$. Performance can still be improved by reducing ρ, but this will decrease the robustness of the closed loop system. This is discussed in the next section.

D. Closed Loop Stability

For internal stability of the close loop system, it is enough to consider the feedback system

$$p_c = P_1 q_c. \tag{32}$$

$$q_c = K_N p_c \tag{33}$$

Now define the nominal open loop plant; $G_{nom}^N(s)$, multiplicative uncertainty; $\Delta_N(s)$, and the sensitivity transfer function $T_N(s)$ s.t.

$$G_{nom}^N(s) = \tilde{P}_1^N(s) K_N(s) \tag{34}$$

$$\big(1 + \Delta_N(s)\big)\tilde{P}_1^N(s) = P_1(s) \tag{35}$$

$$T_N(s) = \frac{G_{nom}^N(s)}{1 + G_{nom}^N(s)} \tag{36}$$

Then a sufficient condition for robustness is [11]

$$|T_N(i\omega)| \leq \frac{1}{|\Delta_N(i\omega)|}, \quad \forall \omega \tag{37}$$

To check this condition $|T_N(i\omega)|$ and $1/|\Delta_N(i\omega)|$ is plotted for $N = 10, 20$ in Fig. 11 and 12. It can be seen that there is a potential lack of robustness for K_{10} as the discretized model

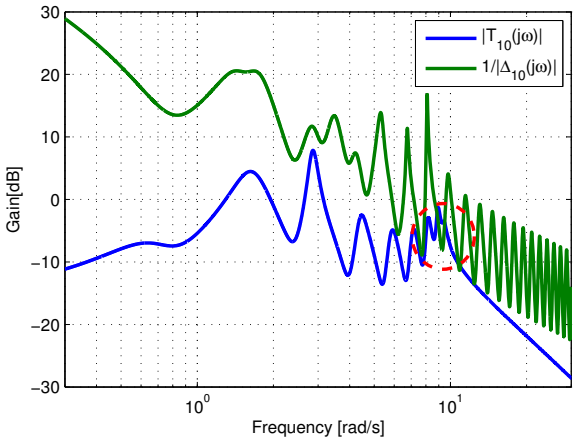

Fig. 11. Checking sufficient condition for robust stability by comparing $|T(i\omega)|$ and $1/|(\Delta(i\omega))|$. For this controller, $N = 10$, there is a potential lack of robustness.

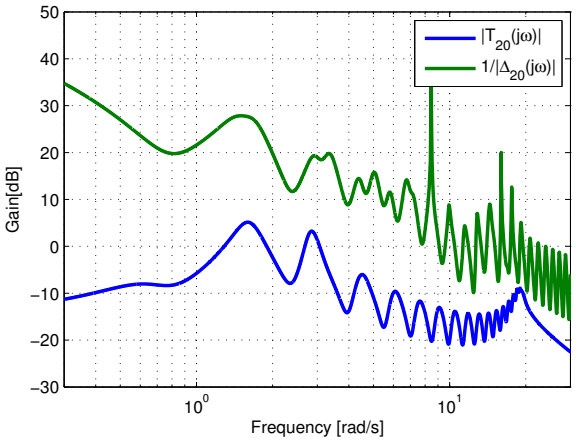

Fig. 12. Checking sufficient condition for robust stability by comparing $|T(i\omega)|$ and $1/|(\Delta(j\omega))|$. For this controller, $N = 20$ Uncertainty is reduced and robustness is ensured.

insufficiently accounts for the resonances around 10 rad/s. When doing controller design with the discretized model it is important to ensure low gain at high frequencies for the nominal open loop plant G^N_{nom} so as to ensure robustness against the un-modelled high frequency resonances in the system. There are a few ways to make the LQG closed loop system more robust. Here we will mention two:

- Reduce the gain of G^N_{nom} at high frequencies by using Frequency shaped LQR with a high pass cost function: $\rho(i\omega)$. (Obviously just increasing ρ without using frequency weighting would also work but may compromise performance).
- Reduce uncertainty by increasing the number of control volumes.

The last point is verified in Fig. 12 where K_{20} is shown to be robust w.r.t. the uncertainty due to the discretization.

ACKNOWLEDGMENT

The first author would like to thank Hessam Mahdianfar of NTNU for valuable suggestions in preparing this paper.

REFERENCES

[1] J.M. Godhavn, P. Alexey, G.O. Kaasa, N. L. Rolland, Drilling Seeking Automatic Control Solutions, in Proc. of the 18th IFAC World Congress, Milano, Italy, 2011.

[2] I.S. Landet, H. Mahdianfar, U.J.F. Aarsnes, A. Pavlov, O.M. Aamo, Modeling for MPD Operations with Experimental Validation, Presented at the IADC/SPE Drilling Conference and Exhibition, San Diego, California, USA, 6-8 March, 2012.

[3] A. Pavlov, G.O. Kaasa, L. Imsland, Experimental Disturbance Rejection on a Full-Scale Drilling Rig, Presented at the 8th IFAC Symposium on Nonlinear Control Systems, Bologna, Italy, 2010.

[4] O. Egeland, J.T. Gravdahl, Modelling and Simulation for Automatic Control, Trondheim, Norway: Marine Cybernetics, 2002, ch 4.

[5] J. Mäkinen, R. Piche, A. Ellman, Fluid transmission line modeling using a variational method, J. Dynamic Systems, Measuremnet, and Control 122, 153-162, 2000.

[6] O.N. Stamnes, J. Zhou, G.-O. Kaasa, O.M. Aamo, , Adaptive observer design for the bottomhole pressure of a managed pressure drilling system, Decision and Control, 2008. CDC 2008. 47th IEEE Conference on , vol., no., pp.2961-2966, 9-11 Dec. 2008 doi: 10.1109/CDC.2008.4738845

[7] G. Kaasa, O.N. Stamnes, L. Imsland, O.M. Aamo, Intelligent Estimation of Dowhole Pressure Using a Simple Hydraulic Model, Presented at the IADS/SPE Managed Pressure Drilling and Underbalance Operations Conf. and Exhibition, Denver, Colorado, USA, 5-6 April, 2011.

[8] O.Breyholtz, G. Nygaard, J.-M. Godhavn, E.H. Vefring, Evaluating control designs for co-ordinating pump rates and choke valve during managed pressure drilling operations, Control Applications, (CCA) & Intelligent Control, (ISIC), 2009 IEEE , vol., no., pp.731-738, 8-10 July 2009, doi: 10.1109/CCA.2009.5281013

[9] H. Mahdianfar, O.M. Aamo, A. Pavlov, Attenuation of Heave-Induced Pressure Oscillations in Offshore Drilling Systems, in American Control Conference (ACC). Montral, Canada: IEEE, June 2012

[10] H. Mahdianfar, O.M. Aamo, A. Pavlov, Suppressing heave-induced pressure fluctuations in MPD, in IFAC Workshop - Automatic Control in Offshore Oil and Gas Production. Trondheim, Norway: IFAC, May 2012.

[11] R. Horowitz, Lecture Notes on LQG Loop Transfer Recovery and Frequency Shaped LQR, Lecture notes from the Course ME233 Advanced Control Systems II, University of California Berkeley, 2011.